

AV RADITSIS

THE INHIBITION OF THE A β OLIGOMERIZATION BY Tf UTILIZING NMR

MSc

UNDERSTANDING THE INHIBITION OF THE AMYLOID- β PEPTIDE
OLIGOMERIZATION BY TRANSFERRIN UTILIZING NMR SPECTROSCOPY

By

ANNIE VICTORIA RADITSIS
BSc.Honours Chemistry, University of Waterloo

A Thesis

Submitted to the School of Graduate Studies

in Partial Fulfillment of the Requirements

for the Degree

Master of Chemistry

McMaster University

© Copyright by Annie Victoria Raditsis, December 2008

MASTER OF CHEMISTRY (2008)

McMaster University
Hamilton, Ontario

Title: Understanding the Inhibition of the Amyloid- β Peptide Oligomerization by Transferrin Utilizing NMR Spectroscopy

Author: Annie Victoria Raditsis, BSc (University of Waterloo)

Supervisor: Associate Professor Dr. Giuseppe Melacini

Number of Pages: IX, 91

Abstract

Understanding the Inhibition of the Amyloid- β Peptide Oligomerization by Transferrin Utilizing NMR Spectroscopy

A hallmark of *Alzheimer's disease* (AD) is the accumulation of insoluble senile plaques in the brain.¹ The major component of the insoluble plaques is the *amyloid- β peptide* (A β) that is produced through cleavage of the *amyloid- β precursor protein* (APP).² It is well understood that once the monomeric A β is generated, it has the potential to aggregate into soluble oligomers and further into insoluble fibrils. Recently it has been proposed that early oligomers are the main toxic species in the aggregation cascade.³ However, it has been shown that the formation of toxic early oligomers is inhibited by several endogenous plasma proteins, including albumin and *transferrin* (Tf). In this investigation we are focusing on the mechanism of inhibition of the A β early oligomerization by Tf. Specifically, we have targeted the early stages of A β aggregation using a deletion mutant of the A β peptide, *i.e.* the A β 12-28 fragment, which selectively stabilizes the early A β oligomers. Self-association of this peptide was controlled by adding-NaCl to filtered monomeric A β samples and the effect of Tf inhibition on these aggregates was probed by ¹H relaxation NMR experiments.⁴⁻⁷ Our data shows that Tf directly targets intermediary A β oligomers via a coating mechanism.

1. Kirkitadze, M.D., Condron, M.M. and Teplow, D.B, *JMB* **2001** 312;1103-1119.
2. Stefan F. Lichtenthaler and Christian Haass, *JCI* **2004** 113(10);1384-1387.
3. Necula M., Kaye R., Milton, S. and Glabe C.G, *JBC* **2007** 282(14);10311-10324.
4. Klement K., Wieligmann K., Meinhardt J., Hortschansky P., Richter W., and Fändrich M., *JMB* **2007** 373;1321-1333.
5. Huang H, Milojevic J, Melacini G. *J Phys Chem B*. **2008** 112(18):5795-802.
6. Milojevic J, Esposito V, Das R, Melacini G. *JACS*. **2007** 129(14):4282-90.
7. Milojevic J, Esposito V, Das R, Melacini G. *J Phys Chem B*. **2006** 110(41):20664-70.

Acknowledgment

I have many people to thank for helping me through the two years of research at McMaster University.

I would like to thank the Canadian Institutes of Health Research (CIHR), the Canadian Foundation for Innovation (CFI), the Natural Sciences and Engineering Research Council of Canada (NSERC), the Alzheimer's Society and McMaster University for providing the necessary funding for this project.

To the McMaster NMR Facility, Dr. Don Hughes, Dr. Steve Kornic and Dr. Bob Berno for all their advice and guidance on NMR, experiments and graduate school.

To Dr. Richard and Raquel Epanand for the use of their CD instrument, but also for their thoughtfulness and overall generosity.

I especially like to thank my supervisor Dr. Guiseppe Melacini. From my initial interview upon applying to graduate school to my final defense he has always kept me inspired to work hard and achieve more.

To my lab group. Julijana Milojevic for all her help and encouragement throughout the entire project. Rahul Das and Soumita Sil for all their knowledge and laughter. Somenath Chowdhury, for treating me like a little sister. Tyler McNichol and Rajeevan Selvaratnam for keeping up good late night conversations. And to all the undergraduate students, especially Elle for keeping me amused during the long hours in the lab.

To my office mates in the Dr. Goward group. Our morning discussion helped start my days. And though their research was in a different field their advice and aid was always much appreciated.

To all my friends within the chemistry department, the ones that went for coffee breaks, baseball games and walks were all necessary for helping me in times of celebration and through the times of distress.

I have to thank my family. My parents, for providing me with everything I could possibly need. My grandparents, for being so understanding and lending me wise words of wisdom. To all my sisters and brothers, Mary, Mike, Elizabeth, Cesar and Nicholas for always looking out for me.

Last, I want to thank Adam. He was always there for me; regardless of if he was physically here or not, it was very apparent that I had the support that I needed to carry on.

Table of Content

Abstract	III
Acknowledgment	IV
Table of Content	V
List of Figures	VIII
List of Schemes	VIII
List of Tables	VIII
Abbreviations	IX
Chapter 1: Introduction	1
1.0 Alzheimer's Disease	2
1.1 The Amyloid beta Peptide	3
1.1.1 The Formation of the Amyloid- β Peptide	4
1.1.2 Location and Concentration of the Amyloid- β Peptide throughout the Body	6
1.1.3 The Length of the Amyloid- β Peptide	7
1.1.4 The Nomenclature of the Oligomeric State	8
1.1.5 The Structure of A β	9
1.2 Oligomerization of the Amyloid-β Peptide	11
1.2.1 Determinants of Self-Association for the Amyloid- β Peptide	12
1.2.2 Nucleation-Dependent Polymerization	13
1.2.3 The Oligomerization Distribution of the Amyloid- β Peptide	14
1.2.4 The Toxic Moiety of A β Aggregation	15
1.3 Hypotheses on Possible Causes of AD	16
1.3.1 The Role of Iron in Alzheimer's disease	16
1.4 Transferrin	18
1.4.1 The Structure of Transferrin	18
1.4.2 Iron Saturated States of Transferrin	20
1.5 Objectives	21
1.5.1 Plasma Inhibitory Protein	22
1.5.2 The Independent Action of Tf	22
1.5.3 A Mechanism of Inhibition	22
1.5.4 The Identification of the Oligomeric A β Species	23
1.6 Protein NMR	24
1.6.1 Nuclear Magnetic Resonance	24
1.6.2 NMR Sample Requirements	25
1.6.3 A β Detection Utilizing NMR	26
Chapter 2: Materials and Methods	30
2.0 Materials	31
2.1 Sample Preparation	31
2.1.1 Preparation of NMR Samples of the A β 12-28 Peptide	31
2.1.2 Protein Sample Preparation	33
2.2 Methods	35
2.2.1 NMR Spectroscopy	35
2.2.2 1D Saturation Transfer Difference (STD) Experiments	37
2.2.3 2D Off-Resonance Relaxation (ORR) Experiment	39
2.2.4 Transfer 2D Nuclear Overhauser Enhancement Spectroscopy (Transfer 2D-NOESY) Experiments	41

2.2.5	Inductively Coupled Plasma Experiments	42
2.2.6	Circular Dichroism (CD) Spectroscopy	42
Chapter 3: Results and Discussion		45
3.0	Sample Preparation for the Focus of Early Aβ Aggregation	46
3.0.1	The Control and Stabilization of the A β 12-28 Peptide Sample	46
3.0.2	Effectiveness of Filtration	47
3.0.3	Influence of Salt on the Aggregation of A β 12-28 peptide	49
3.1	Verification of Tf's Involvement with the Aβ12-28 Peptide Sample	50
3.1.1	The ability of Tf to Disrupt the Dynamic Exchange between Monomeric and Oligomeric States of A β 12-28	50
3.1.2	The Distribution of A β Aggregation with Respect to Pre-Nuclear A β Oligomers in the Presence of Tf	53
3.2	The Involvement of Iron and Tf in the Inhibition of Aβ12-28 Aggregation	55
3.2.1	The Inhibition of A β Aggregation by Tf Not Iron Mediation	55
3.2.2	Each Degree of Iron Saturation of Tf possesses Inhibitory ability on the Aggregation of A β 12-28	57
3.2.3	The Effect of Residual Iron within the Sample	60
3.3	Quantifying the Binding Potencies and the Mechanisms for the Tf, Aβ12-28 Interactions	61
3.3.1	Tf Does Not Interact with Monomeric A β Peptides.	61
3.3.2	Quantitative Investigation of the Interactions between A β 12-28 and Tf through 1D 1H-STD NMR Experiments	63
3.3.3	Tf Shields All Residues of Monomeric A β 12-28 from Their Interactions with A β 12-28 Oligomers	65
3.4	The Mechanism for the Inhibition by Tf of the Aβ12-28 Oligomerization	67
3.4.1	Tf Inhibits the Early A β Oligomerization through a Competitive Mechanism	67
3.5	The Structural Analysis on the Intermediates Targeted by Tf for the Inhibition of Aβ12-28	69
3.5.1	Secondary Structural Analysis through 2D NOESY NMR Experiments	69
3.5.2	Analysis of A β Oligomeric Binding to Tf through CD Spectroscopy	72
Chapter 4: Conclusions		74
4.0	Tf Inhibits Early Oligomerization in the Aβ Self-Association Process and Key Determinates of Inhibition are Contained within the 12-28 Region of the Aβ Peptide	75
4.1	The Inhibitory Effect of Tf on Early Aβ Aggregation is Not Iron Mediated	75
4.2	The Degree of Iron Saturation in Tf Does Not Significantly Affect the Tf Inhibitory Potency	76
4.2.1	The Potency of the Inhibition of A β Oligomerization is Below the Reported Tf Concentration in CSF	77
4.3	Tf Utilizes a Competitive Mechanism for the Inhibition of the Early Stages of Aβ Oligomerization	77
4.3.1	The Mechanism of Inhibition Does Not Imply the Destabilization of A β Oligomeric Intermediates	78
4.3.2	Tf Does Not Interact with the Monomeric Portion of A β	78
4.3.3	Oligomeric Concentration Dependence is Exhibited for Tf Inhibition	78
4.4	All Amino Acid Residues in the Oligomeric Species are Entirely Shielded by the Inhibitory Mechanism of Tf	79

Chapter 5: Future Work	80
5.0 Investigation of Iron - A β 12-28 Binding	81
5.1 Relevance of Inhibition upon the involvement of A β 42	82
5.2 Verification of Apo-Tf and Holo-Tf Species	83
5.3 Utilization of Various Detection Techniques to Expand the Limit of Detection	83
5.4 Determination of the Specific Binding Sites	84
5.5 Comparison to Other Common Plasma Proteins	85
References	86 - 91

List of Figures

1.1	Outline of the A β -Domain within the Integated-Membrane Protein APP	4
1.2	The Amyloidogenic and No-Amyloidogenic Pathways of APP	6
1.3	Defining Terminology for A β Aggregation	9
1.4	Nucleated Polymerization of the On and Off-Pathways of the A β -Fibril Formation	14
1.5	The Location of High Affinity Metal Binding within A β	17
1.6	The 3D Structure of Porcine Serum Transferrin	20
1.7	A Hypothesized Competitive Mechanism for the Inhibition of A β Aggregation by Tf	23
1.8	The Mechanism of Saturation Transfer Difference Experiments	28
2.1	1D ¹ H-WG NMR Pulse Sequence	36
2.2	1D ¹ H-STD NMR Pulse Sequence	37
3.1	1D ¹ H-WG Spectral Detection of the Aggregation of A β 12-28	47
3.2	The Observation of ‘Cake Effect’ Through Filtration of A β Peptide Samples	48
3.3	The Stabilization Periods Associated with the Addition of Salt to the A β Peptide Sample	49
3.4	1D ¹ H-WG Spectral Comparison of Interactions of Tf with the A β 12-28 Peptide	52
3.5	The Effects of Progressive Aggregation on A β with the Involvement of Tf	54
3.6	The Sequestration of Iron and it Implications to the Tf Inhibitory Mechanism	57
3.7	The Various Degrees of Iron Saturation for Tf and Their Potency for the Inhibition of the A β 12-28 Peptide	58
3.8	Probing the A β Inhibitory Abilities of Tf at Various Degrees of Iron Saturation	59
3.9	Determination of Monomeric A β /Tf Binding Contributions	62
3.10	Changes Induced with the Introduction of Tf to Aggregated A β Samples	64
3.11	The Global Shielding on A β 12-28 Intermediates by Tf	66
3.12	The Two Most Probable Mechanism for the Inhibition of A β Aggregation by Tf	67
3.13	Tf Does Not Destabilize Oligomeric A β Intermediates	69
3.14	Structural Analysis of Targeted Intermediate in A β Inhibition	71
3.15	CD Spectroscopy for Structural Analysis upon Aggregation and Inhibition of A β	72

List of Schemes

I	Verification of the Interaction of Tf and the Amyloid- β Peptide through 1D ¹ H-WG NMR	51
II	Salt Titration to Mimic the Aggregation Process of A β	53
III	The Comparison between Inhibitory Mechanisms of EDTA and Tf for A β Oligomerization	56
IV	Titration of Tf against Monomeric and Oligomeric Samples of A β	63

List of Table

1.1	The Locations and Concentration of the Various States of Tf	21
-----	---	----

Abbreviations

1D	1 Dimensional
2D	2 Dimensional
AD	Alzheimer's Disease
ADDLs	A β derived diffusible ligands
AICD	APP Intracellular Domain
AIHA	American Industrial Hygiene Association
ApoE	Apolipoprotein E
Apo-Tf	Iron-Free Transferrin
APP	Amyloid Precursor Protein
A β	Amyloid- β Peptide
BACE	β -Site APP Cleaving Enzyme
BBB	Blood Brain Barrier
BCA	Bicinchoninic Acid
BSA	Bovine Serum Albumin
CD	Circular Dichroism Spectroscopy
CNS	Central Nervous System
CSF	Cerebrospinal Fluid
CTF- β	Carboxyl C-Terminal Fragment
Da	Daltons
EDTA	Ethylenediaminetetraacetic Acid
FAD	Familial Alzheimer's Disease
FID	Free Induction Decay
FT	Fourier Transform
Holo-Tf	Diferric Transferrin
IC ₅₀	Half-Maximal Inhibitory Protein Concentration
K _d	Dissociation Constant
kDa	KiloDaltons
MS	Mass Spectrometry
MHz	Mega Hertz
NFT	Neurofibrillary Tangles
NMR	Nuclear Magnetic Resonance
NOE	Nuclear Overhauser Effect
NOESY	Nuclear Overhauser Effect Spectroscopy
NRMS	Normalized RMS Deviation
OD	Optical Density
ORR	Off Resonance Relaxation
PFs	Protofibrils
PII	Polyproline II
RF	Radio Frequency
RIP	Regulated Intermembrane Proteolysis
RMSD	Root Mean Squared Deviation
SL	Spin-Lock Filter
STD	Saturation Transfer Difference
STR	Saturation Transfer Reference
TOCSY	Total Correlation Spectroscopy
Tf	Transferrin
TfR	Transferrin Receptor
ThT	Thioflavin T
Watergate or WG	Water Suppression by Gradient-Tailored Excitation

Introduction

Chapter 1

Introduction

1.0 Alzheimer's Disease

Alzheimer's disease (AD) was first established in 1907 by the German physician Alois Alzheimer in the course of a neuropathological study involving a 51-year old woman's brain.¹ These findings initiated the association of AD with *neuritic plaques* (extracellular insoluble amyloid-beta aggregates) and the *neurofibrillary tangles (NFT)*, intracellular lesions consisting of paired helical filaments formed of hyperphosphorated cytoskeletal protein τ).²⁻⁵ However, the pathogenesis of this neurodegenerative disease has remained elusive for many years until the senile plaques were further explored, resulting in the purification of the *amyloid beta peptide (A β)*. Once A β was identified, the premise of an imbalanced metabolism of A β initiating aggregation and further leading to the formation of *neuritic plaques* was deduced.

The abnormal oligomerization or mis-folding that distinguishes AD also describes a number of other diseases namely; Creutzfeldt-Jakob disease, Huntington's disease, Parkinson's disease and type II diabetes.^{2,3,6} These groups of disorders are typically referred to as *conformational disorders*, due to their conformational changes observed during aggregation.^{4,7,8} Due to its relevance to many diseases, the study of the protein aggregation, bio-physical chemistry has been intensified within the past decade.

AD is clinically characterized as a combination of progressive, cognitive and memory deficits caused by a more generalized cortical atrophy, starting in the medial temporal lobe.⁷ AD has been recognized in two forms: *familial Alzheimer's disease*

(FAD) and *sporadic AD*. A hereditary component influences both types of AD. FAD is linked to point mutations within the A β -domain of APP as well as known mutations within presenilins (1 and 2) which lead to an increased production of A β and therefore accelerating of plaque pathology.⁹ The majority of AD cases reported are the late onset of *sporadic AD*, which develops after the age of 65 though the cause is uncertain. It is thought to be associated with an increased risk of *apolipoprotein E (ApoE)*, ϵ 4 allele genetic damages that attribute to A β deposition.¹⁰

Existing treatments for the disease are symptomatic-based, including cholinesterase inhibitors and glutamate-modulating drugs as the most advanced treatments.³ Although useful, these symptomatic treatments do not prevent neuronal degeneration and death. Considering the increasing rate of incidence for AD among the aging population further research is greatly required.

1.1 The Amyloid beta Peptide

Amyloid is a generic name for insoluble fibrillar protein deposits that are formed *in vivo*. This fibril formation is remarkably similar throughout the various *conformational disorders*, despite the varying nature of the proteins involved. Typically, fibrils are resistant to degradation and bind dyes such as *thioflavine T (ThT)* and *Congo red*. Amyloids are found in two distinct forms; local, in a particular tissue or systemic, in many organs around the body. The most common form is local, which is found in the *central nervous system (CNS)*, the cardiovascular system, or in some endocrine organs.

1.1.1 The Formation of the Amyloid- β Peptide

The A β peptide originates from the *amyloid- β precursor protein* (APP), a 695-amino acid glycoprotein which is firmly linked to AD through genetic studies involving the mutation of presenilins 1 and 2. Presenilins are central components in the cleaving enzymes involved in the formation of A β .⁷ APP is a occurring type I integrated membrane protein containing the A β -domain which is situated in both intermembrane and extracellular regions¹¹ (Figure 1.1). APP is synthesized in the endoplasmic reticulum and is involved in cell adhesion, neurite outgrowth, synaptogenesis and synapse remodeling.¹²

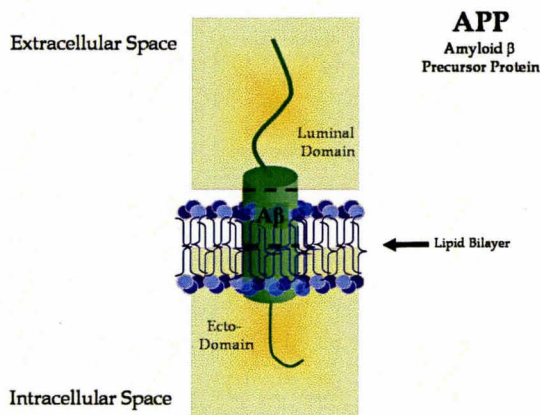


Figure 1.1 | Outline of the A β -Domain within the Intergated-Membrane Protein APP | APP is a glycoprotein that encompasses the A β domain in both the intermembrane and extracellular regions. The AD-related peptide lies within the membrane and in the luminal domain that is situated with residue 1-18 in the extracellular space (as seen with the dashed lines) and the remaining 19-40/42 within the lipid bilayer. Knowledge of the APP within the body has been linked to transcriptional messaging, though a definite role has not been clarified.

The cleavage of APP to release A β is known as the *regulated intramembrane proteolysis* (**RIP**). The product resulting from RIP is known to contain A β (Figure 1.2),

though the properties of the proteolytic mechanism remain unclear.¹¹ RIP involves sequential cleavage by β - and γ -secretase.¹¹ The initial cleavage is generated by β -secretase (*β -site APP cleaving enzyme, BACE*), composed of a complex of proteins (presenilin 1/2, nicastrin, APH-1 and PEN-2).¹¹ Upon BACE cleavage at residues 596 and 597 of APP, the generation of a C-terminus 99 amino acid chain, known as the membrane-bound *C-terminal fragment (CTF- β)* releases the large luminal domain into the extracellular space.¹¹ Subsequently, γ -secretase mediates the intramembrane cleavage of CTF- β at residual 38, 40 or 42 resulting in the formation of a cytoplasmic fragment, known as the APP intracellular domain (**AICD**) and the release into the extracellular space.¹¹ AICD starts at position 49/50 and would not correspond to the end of the A β variants A β 40 and A β 42. Recently, an additional ϵ - cleavage that occurs near the membrane–cytoplasm boundary, beyond the γ -cleavage sites to generate longer A β within cells and in the brain, including A β 43, 45, 46 and 48.¹³ However the function and relevance of the longer A β chains have yet to be discovered. There is also an alternative and non-amyloidogenic pathway for APP cleavage (Figure 1.2). This cleavage occurs at Lys16 – Leu17 within the A β -domain of APP by α -secretase resulting in a soluble C-terminus 83 amino acid peptide chain, known as the membrane-bound α -APP in the ectodomain. This resulting peptide chain is further cleaved by γ -secretase to produce CTF- β and the remaining A β -domain, Leu17 - Gly38, or Leu17 - Val40, or Leu17 - Ala42.¹¹

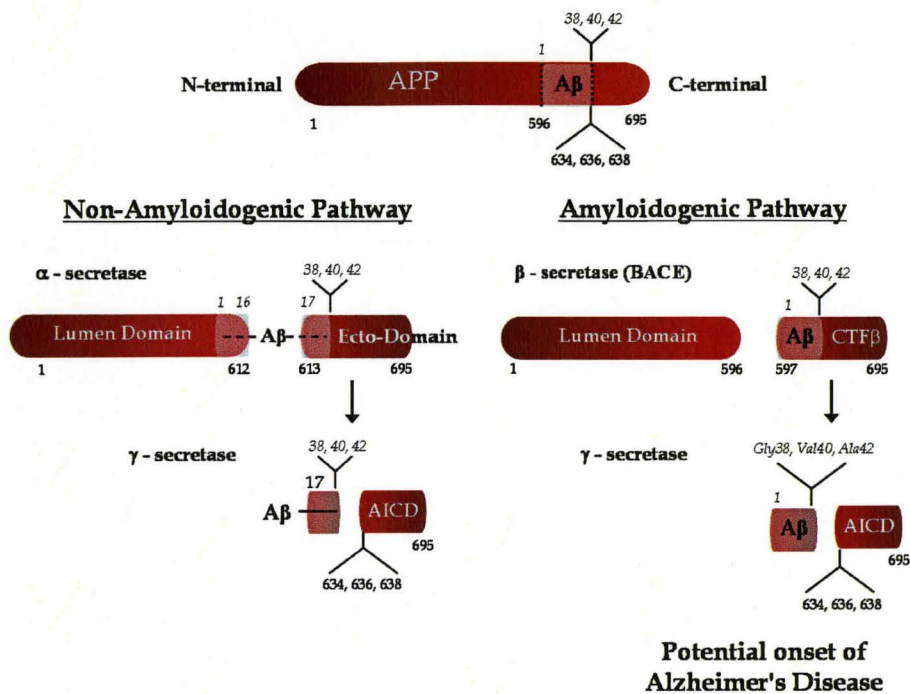


Figure 1.2 | The Amyloidogenic and Non-Amyloidogenic Pathways of APP | The regulated intramembrane proteolysis (RIP) generates A β utilizing; β -site APP-cleaving enzyme (BACE) and γ - secretase to cleave APP to release A β into the extracellular space. The isolation of A β in the extracellular space enables A β aggregation, this is known as the amyloidogenic pathway, leading to the formation of senile plaques. The alternate, non-amyloidogenic pathway involves RIP through the use of α - and γ - secretases to cleave APP between the 16th and 17th residues of APP in the A β domain thus inhibiting the formation of A β and further senile plaque formation.

1.1.2 Location and Concentration of the Amyloid- β Peptide throughout the Body

A β has been observed as a regular constituent in plasma under normal physiological conditions. It has been detected in conditioned media of various tissue culture cell lines suggesting that it is produced and secreted constitutively throughout the body.¹⁴⁻¹⁶ Although most cells in the body contains A β , a physiological function for the peptide has yet to be determined. The circulating pool of A β within the body is produced by peripheral tissues and organs.¹⁷ Published concentrations for A β in plasma are

reported as the mean value at 150 pM for A β 40 and 20 pM for A β 42.¹⁸ In the CSF an increase of concentration were reported at a mean value of 625 nM for A β 40 and 60 pM for A β 42 respectively.¹⁹ Under normal physiological conditions, the concentrations are typically found six-fold higher within the CSF in comparison to the plasma.¹⁷

1.1.3 The Length of the Amyloid- β Peptide

The two most abundant forms of A β generated by RIP are A β 40 and A β 42. The sequence of the two differs by two amino acids, though there are great characteristic differences between them. A β 40 is the predominant species *in vivo*, approximately 90% of all A β normally released from cells. However, the 10% of A β 42 is more amyloidogenic, providing a major contribution to the formation of neuritic plaques.^{20,21} The soluble form, A β 40, is stable for up to 1-2 days, whereas A β 42 aggregates instantly, reinforcing the fact that A β 42 is the more toxic species.^{15,22} Differences in aggregation of the two peptides may be derived from the different exposure of the hydrophobic residues. Since A β 42 has more exposed hydrophobic residues it preferentially forms intermediary oligomers at an increased rate. Small molecular weight oligomers are characterized as dimers – octamers, while high molecular weight oligomers correspond to containing 20 – 40 monomers.²³ Both A β types play a role in AD, as high concentrations of both A β 40 and A β 42 within the CSF (~10 fold in comparison to healthy tissue) have been shown to correlate with AD plaque formation.²

1.1.4 The Nomenclature of the Oligomeric State

In order to fully describe the oligomerization process of A β , the structural intermediates that are formed need to be classified. Small soluble oligomers are found *in vivo* the CSF of both healthy and AD tissue. The list of types of assemblies identified for A β are: protofibrils (PFs), annular structures, paranuclei, A β -derived diffusible ligands (ADDLs), globulomers, A β *56 and amyloid fibrils. The intermediates termed annular structures, paranuclei and globulomers have only been deduced through *in vitro* techniques and their physiological relevance has yet to be determined. The remaining intermediates have been identified as *in vivo* intermediates and has been associated with the formation of toxic fibrils.

Electron microscopy A β 42²⁴ and A β 40²⁵ showed that later-stage oligomers adopted a larger oligomeric structure, known as the ADDLs, which have been reported to be toxic to the neurons and linked to the induction of cognitive memory loss related to AD. These oligomeric intermediates have been isolated *in vivo* at an increased concentration of 70-fold upon the onset of AD.²⁶ Another *in vivo* intermediate, isolated in transgenic mice is A β *56.²⁴ Identified for the aggregation of both A β 42 and A β 40 peptides, it is characterized by a dodecamer of the A β peptide.²⁷ This intermediate has been observed within the development of senile plaques playing a key role in memory deterioration.²⁸ PFs are larger oligomers that adopt a structure that is narrower than the *bona fide* amyloid fibrils that also adopts a β -sheet that binds to ThT.²⁹ Recently, elevated levels of A β protofibrils have been found before the appearance of plaque pathology in

transgenic mice.³⁰ Figure 1.4 provides a description of the aggregation pathway and terminology that will be used throughout this report.

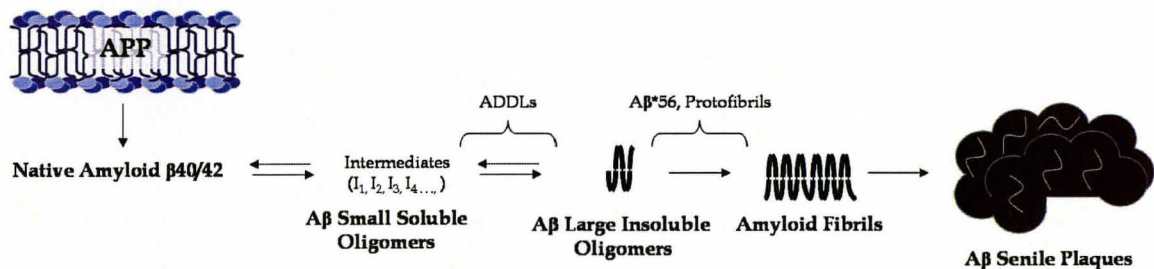


Figure 1.3 | Defining the Terminology for A β Aggregation | The identification of the distribution of A β intermediates is one of the challenging aspects in studying A β aggregation. To clarify the work that has been done on the detection of specific intermediates *in vivo*, an outline of a potential aggregation map is laid out following the *Amyloid Cascade Hypothesis*.

1.1.5 The Structure of A β

The specific sequences of A $\beta_{40/42}$ can be classified into domains based on the structure, charge, polarity and hydrophobicity. Residues Asp1 - Lys16 are the polar N-terminus, have minimal to no impact on aggregation.³¹ The most structured region incorporates residues Glu22 – Lys28,³² and residues that have been linked to aggregation due to their hydrophobic nature are Leu17 – Ala21. Ile31-Ile32 and Val39 – Val40/Ala42 are also hydrophobic regions.³³ These regions of the peptide have also been shown to be consistent for segmented variations of the full-length peptide, specifically A β_{10-35} ³⁴ and A β_{12-28} .³⁵

Amyloid fibrils of A β 40/42 have been defined as β -strand enriched fibrils organized into unbranched β -sheets at 7 - 10 nm.³⁶ Most structural elucidation of A β 40/42 has been performed using solid-state NMR. The monomeric domains of A β within fibril formation adopts a bend in residues Glu22 – Gly29³⁷ in order to create a hydrophobic contact with the β -strand regions of Val12-Ala21 (β 1) and Val30-Val40/Ala42 (β 2)^{36,38}, enforced by the formation of a salt bridge by ionic amino acid Asp23 and Lys28.³⁶ The stacking of A β 42 is known to lead to the formation of hydrophobically-driven β -sheet protofibrils, approximately 5.5 nm wide and 1.5 nm high that intertwine to form helical insoluble fibrils.³⁹

A β 12-28 has been used as a model for early aggregation. In order to understand the mechanism of peptide aggregation it is important to understand the structure of the monomeric form of the peptide. Initial studies of A β 12-28 suggested a random coil structure, however with further studies it was only found at low (< 280 K) temperatures and gradually converted to a left-handed 3_{10} -helix, polyproline II (PII).⁴⁰ Several reports since then have combined simulations with experimental results to show that A β 12-28 at 280 K co-exists with PPII, β -strand and β -turn structures.⁴¹ The highest population of PPII states is observed in the central Ala21, Glu22 and C-terminal Ser26, Asn27 regions of the peptide. A high propensity to form β -strands is observed for residues Phe20 and Val24 and to a lesser extent His14-Leu17. These two β -strand regions are connected by a β -turn at Val18 and Phe19, suggesting the presence of a β -hairpin conformation.⁴¹ Within the A β 12-28 it is also reported that the lowest energy conformation has

hydrophobic contacts between V12 and V24, which results in the reduction of the exposed hydrophobic surface and also provides stabilization for the proposed β -hairpin conformation.⁴⁰

Upon temperature-induced aggregation, the two phenylalanines in the central hydrophobic cluster, Phe19 and Phe20 were reported to have a β -strand conformation,⁴² indicating that this peptide fragment has a dependence on residues Phe19 and Phe20 for aggregation. These results were reinforced through mutation studies to remove one or both of the targeted residues, which resulted in a significant decrease of aggregation. The A β 12-28 fragment contains the key residues which enable aggregation and it is an appropriate model of the early stages of the full-length A β 40/42 aggregation.⁴⁰

1.2 Oligomerization of the Amyloid- β Peptide

The general model of A β aggregation as a causative mechanism for AD pathogenesis has been coined the *Amyloid Cascade Hypothesis*, which is based on an imbalance between the production and clearance of A β to form amyloid deposits within the brain⁴³ (Figure 1.3). Starting with the monomeric form, oligomerization commences spontaneously with a transition to a globular-like structures referred to as small soluble oligomers.⁴⁴ This progresses until the aggregation of soluble oligomers become irreversible, forming larger insoluble A β oligomers. Upon further self-association, A β fibrils form rigid β -sheet structures. The accumulation of fibrils, results in senile plaques in the brain. Neurons that are exposed to the newly formed A β fibril/plaque experience extensive oxidative stress that many lead to cellular damage and death.^{43,45}

1.2.1 Determinants of Self-Association for the Amyloid- β Peptide

Aggregation is affected by two major determinants: intrinsic characteristics and the physical-chemical environment. The intrinsic characteristics include hydrophobicity, charge, polarity, aromaticity and β -sheet propensity. Two hydrophobic regions are situated within the A β -sequence: the central region Leu17 - Ala21 and the C-terminal region, Ala31-Val40/Ala42. The central hydrophobic region provides the main driving force for A β self-association and is commonly referred to as the *central hydrophobic core* (CHC). Evidence for such a great effect on aggregation due to hydrophobicity has been outlined by mutagenesis studies.³³ The most dramatic mutation observed is Phe19Asp, which reduces the propensity for the self-association of A β .⁴⁶ This correlates with the high relative aggregation propensity reported for the CHC region of the peptide in comparison to other amino acids.⁴⁶

The other determinant of aggregation is the physical -chemical environment of the peptide/protein, which includes the pH, temperature, ionic strength, agitation, hydrostatic pressure, solvents, and concentration. The influence of pH has been most investigated. A β aggregation is known to be driven by hydrophobicity from the CHC, but also upon the formation of salt bridges involving His residue 3,13,14 and the Arg/Glu carboxylic acid side chains residues D1, E3, D7, E11, E22 and D23.⁴⁷ The formation of salt bridges is dependent on the charge associated with the involved residues, which is controlled by the pH of the environment. The charge of each amino acid is also affected by the attraction required for the formation of anti-parallel β -sheet aggregates. Basic, neutral

and acidic pHs were tested for aggregation propensity on various lengths of the A β peptide. Basic conditions resulted in the lack of fibril formation for all lengths of A β , while a neutral pH allowed for the formation of amyloid-like fibrils and acidic conditions showed a decreased development of fibril fragments.⁴⁷

1.2.2 Nucleation-Dependent Polymerization

Though the detailed mechanism of A β self-assembly is unknown, the A β fibril formation has been hypothesized as a *nucleation-dependent polymerization*.^{48,49} (Figure 1.3) This mechanism is a generalized formula that has been implemented for other known cases of aggregating matrices. The mechanism follows a two-step process starting with the *lag phase*. This is where the initial build-up of soluble oligomers occurs: therefore no apparent fibrils are detected. The lag phase involves the formation of a *critical nucleus*, which is the assembly of aggregates into oligomeric states and corresponds to the largest free-energy barrier species. After this point, the favourable free-energy elongation results in an elevated polymerization for the formation of insoluble oligomers and the development of mature fibrils.

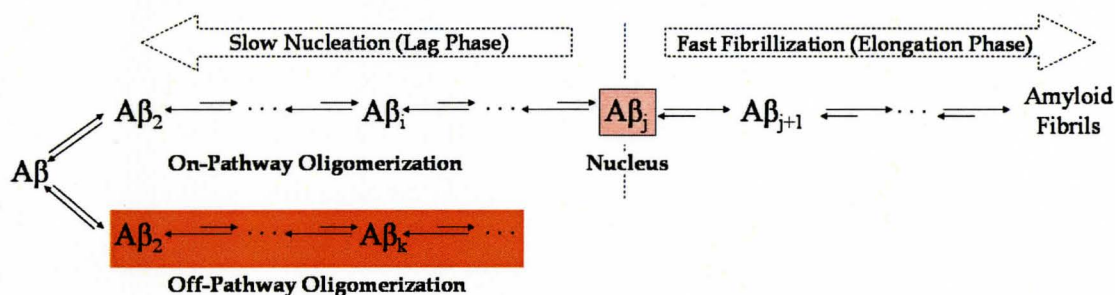


Figure 1.4 | Nucleated Polymerization of the On and Off Pathways of the Aβ-Fibril Formation | Nucleated polymerization has been used to describe many peptide aggregation processes present within the body. Upon the formation of Aβ, the process undergoes a lag-phase that determines the rate of aggregation, The completion of this phase is considered with the formation of the critical nucleus. At this stage aggregation is carried out at a faster rate, this phase is known as the elongation phase. Possible off-path formation of Aβ-oligomers is also possible, up to the formation of a non-toxic aggregates. This pathway is highly unknown, yet may have an influence on the toxic oligomerization pathway.

The polymerization process has been exhaustively researched as an *in vitro* mechanism for Aβ aggregation. Investigation of an off-pathway mechanism has been considered, which may lead to aggregation, but lacks the capabilities of fibril and plaque formation and cellular damage.⁵⁰ Another aspect is the concentration dependence of the mechanism. It has been demonstrated that lower peptide concentrations increase the lag phase.⁵¹

1.2.3 The Oligomerization Distribution of the Amyloid-β Peptide

Along with the change of solubility there are notable conformational changes that occurs during Aβ aggregation. As part of APP, known as the Aβ domain, Aβ_{40/42} contains both extracellular and transmembrane regions. Prior to liberation the peptide

exists in a helical formation. After A β is ejected into extracellular space, the peptide accumulates and spontaneously aggregates into oligomers and fibrils, which is a reported β -sheet formation.⁵² These findings suggest that the process of A β aggregation requires conformational transitions with minimal transition from α -helical to β -sheet.⁴¹

Unfortunately the mechanisms for the structural change that occur from the transformations from monomeric to fibrillar states are still enigmatic. Circular dichroism (CD) spectroscopy has been used to monitor the secondary structures of the full-length peptide and an increase of α -helicity within the early stages of oligomerization was noted.⁵³ With this evidence it was proposed that the A β monomer associates into oligomers in such a way that the hydrophobic tails of the peptides become shielded from the solvent by structural reorganization of the remainder of the peptide.⁴¹ This creates a local apolar micro-environment that promotes growth of helical structures from the pre-existing *seed* or *critical oligomer*.

1.2.4 The Toxic Moiety of A β Aggregation

Much of the current research on AD involves soluble forms of aggregated A β and their potential role as the primary neurotoxic species. Initial investigation on amyloid oligomerization associated A β toxicity with the formation A β fibrils. More recent investigations revealed that soluble A β oligomer concentrations correlated with the observations of dementia more than insoluble A β fibrillar deposits. This holds true for the ADDL intermediates isolated *in vivo*, suggesting that perhaps the soluble oligomeric species of A β are indeed the toxic moiety of AD. Further studies have shown a 70-fold

increase in concentration of oligomers, ADDLs during the progression of AD relative to a healthy brain.²⁶

1.3 Hypotheses on Possible Causes of AD

There is a multitude of possible biochemical alterations linked to AD. Many of the changes have been discovered only upon the onset of the disease, making the distinction between *cause and effect* highly problematic. Early-age FAD has been linked to genetic mutations of the APP that increases the rate of A β formation as well as causing a disruption with the balance of regular brain constituents –*i.e.* hydrogen peroxide, transition metals.^{2,3,5} AD has also been strongly linked to oxidative stress, which is defined as an imbalance between the production of free radicals and the ability of the cell to defend against them through antioxidants and detoxifying enzymes (superoxide dismutase and catalase). Increasing evidence has associated oxidative stress with the modulation of activity and levels of key enzymes involved in the formation of A β with the onset of AD.⁵⁴ This has been linked to the early stages of aggregation, enforced by the observed increase of cellular hydrogen peroxide (H₂O₂).⁴⁵

1.3.1 The Role of Iron in Alzheimer's disease

Iron has been linked to oxidative stress and neurotoxicity within the brain and a reported 50% increase in concentration within the region of senile plaques.⁵⁵ A β 40/42 contains redox-active metal binding sites: His6, His13 and His14 which are located at the

hydrophilic N-terminus of the peptide⁵⁶ and more recently established, Tyr10.⁵⁷ (Figure 1.5)

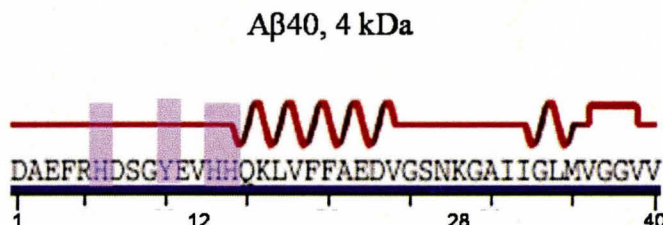
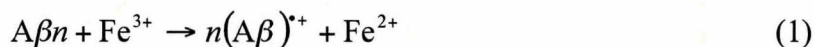
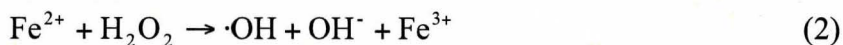


Figure 1.5 | The Location of High Affinity Metal Binding within Aβ | Redox active metals have been a focus of AD research as a potential cause of the disease or a consequence of the onset of the disease. Binding of metal ions: Zn²⁺, Cu²⁺ and Fe³⁺ are experimentally known to promote Aβ oligomerization. The metal binding sites: His6, Tyr10, His13 and His14 are highlighted in the full-length Aβ40 peptide. (Secondary structure for Aβ40 was obtained from the ProteinData Bank)⁵⁸

The generation of hydrogen peroxide by Aβ is thought to involve a formation of a metal:peptide complex. It is proposed that Aβ interacts with molecular oxygen through an electron-transfer to ferric iron to form a peptide radical intermediate, which may lead to cellular damage.



Oxidative stress can also arise from the newly formed ferrous iron based on a cycle between reduced and oxidized states allowing the transfer of electrons to the oxygen of hydrogen peroxide through the Fenton reactions.



The observation of oxidative stress by both Aβ and iron in the CSF results in biomolecular damage and/or death as well as the enhancement of Aβ aggregation.

Iron is well known to have many complex roles throughout the body. In particular, mitochondrial iron is incorporated into heme and cytochromes to transduce the signal of neurotransmitters.⁵⁹ Given the importance of iron in a multitude of metabolic processes, it is understandable that the regulation of iron would also be highly sophisticated and any deregulation would result in detrimental consequences for neuronal function.⁶

1.4 Transferrin

Transferrin (Tf) is a glycoprotein that regulates homeostasis of free iron within the body. Iron uptake in the brain is controlled by the Tf-receptor (TfR), predominately in endothelial cells.⁶⁰ Iron storage is controlled by ferritin, which is found in most CNS cells and keeps iron in a redox-inactive state.⁶¹

1.4.1 The Structure of Transferrin

Iron transport by Tf is carried out by two metal binding sites that have a high affinity for ferric iron, K_a at a range of $1 - 6 \times 10^{22} \text{ M}^{-1}$.⁶² It is composed of 679-residues (MW ~74.5kDa) with two main domains: an amino-terminal domain (N-domain) consisting of residues 1 - 331 and a carboxyl-terminal domain (C-domain) including residues 339 - 679.⁶³ (Figure 1.6) An unstructured linker chain of residues 332 – 338 connects the two domains creating a deep hydrophobic site.⁶³ Each domain is further divided into two sub-domains each containing discontinuous sections of amino acid chains. The first sub-domain within the N-domain is NI made up of residues 1 – 92 and

247 – 331 and connected by NII containing residues 93 – 246, whereas the C-domain contains CI with residues 339 – 425 and 573 – 679 and joined by CII with residues 426 – 572.⁶³ The two domains are equipped with a binding site for ferric iron and a carbonate anion. The two metal binding sites are located at the bottom cleft of each domain.⁶² The domains are have 54% sequence identity and similar functions.^{63,64}

Iron is coordinated by four conserved amino acids: a tyrosine at the hinge site of the NII (CII) sub-domain, another tyrosine within the NII (CII) sub-domain, an aspartic acid playing a key role in the NI (CI) sub-domain, and a histidine at the hinge site of the NI (CI) sub-domain. Fe binds to Tf only in the presence of an anion, typically carbonate, which serves as a bridging ligand between the metal and the protein and excludes water from two coordination sites. Furthermore a *second shell*, an extensive network of hydrogen bonds surrounding the metal binding site involves Gly65, Glu83, Tyr85, Arg124, Lys206, Ser248 and Lys296.⁶⁵ The two lysines found in the *second shell* are thought to act as a *dilysine trigger*, which is proposed to modulate the opening and closing of the sub-domain upon pH fluctuation to release the iron.⁶⁶

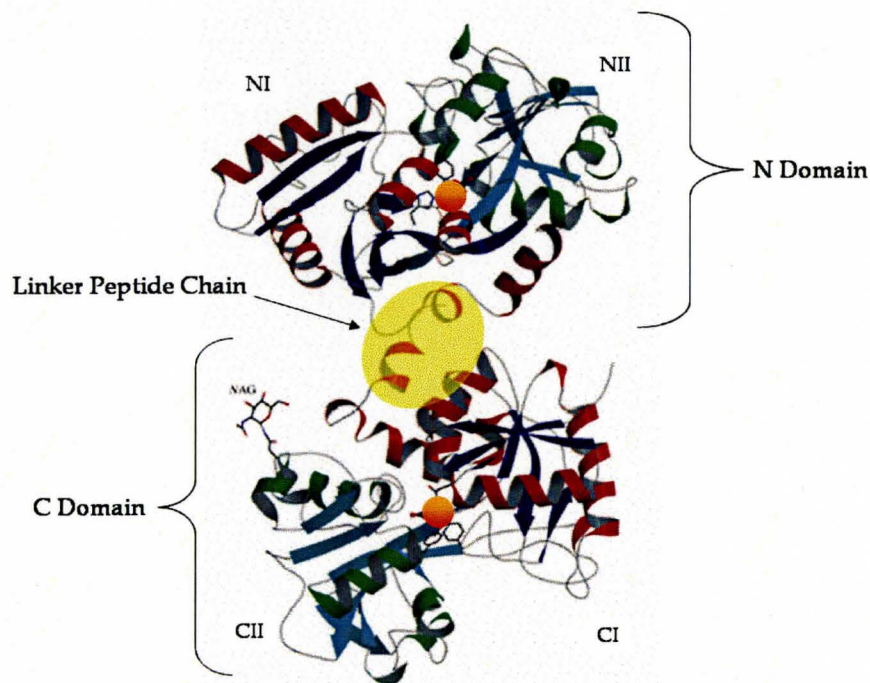


Figure 1.6 | The 3D Structure of Porcine Serum Transferrin | The 679-residue Tf structure contains two domains, N-lobe and C-lobe, which both contain sub-domain arrangements where NI and CI (red and blue) are equivalent, as NII and CII (green and cyan) correspond. Bound iron (orange spheres) and carbonate are also shown in the bottom cleft of each domain. The linker chain, indicated in yellow is the unstructured peptide chain that joins the two lobes together. The structure of transferrin has been shown to be highly similar throughout various species of vertebrates, all of which have an extremely high affinity to ferric iron. This structure was determined with a resolution of 2.15Å.⁶⁷

1.4.2 Iron Saturated States of Transferrin

Several families of transferrins are known to exist in physiological fluids of mammals. Lactoferrin is found in milk, tears and saliva, and Tf is known to be found in the plasma and cerebral spinal fluid (CSF).⁶⁸ Human serum transferrin (**hTf** or **Tf**) exists in two major states: the diferric bound state (**holo-Tf**) and the iron-free state (**apo-Tf**). The monoferric state of Tf has been identified, but has yet to be isolated *in vivo*.

Normally, in the plasma Tf exists at a concentration of $\sim 38 \mu\text{M}^{69}$ with $\sim 40\%$ in the holo state. In the CSF the concentration of Tf is decreased significantly to $\sim 170 \text{ nM}^{69}$ with $\sim 80\%$ in the holo state (Table 1.1). Holo-Tf is known to have a greater affinity for TfR than to the apo-Tf form with a dissociation constant (K_d) of 7 nM (pH 5.0)⁷⁰ versus the K_d for apo-Tf at 13 mM (pH 5.0).⁷⁰

Location	[Tf] / μM	Apo-Tf / %	Holo-Tf / %
Plasma	38^{69}	60 - 70	30 - 40 ⁷¹
CSF	0.17^{69}	20 - 30	70 - 80 ⁶⁰

Table 1.1 | The Locations and Concentrations of the Various States of Tf | Transferrin is not known to cross the BBB (blood brain barrier); instead it is produced both in the plasma and the CSF individually. The concentrations between plasma and CSF are dramatic but both are highly important for the homeostasis of iron in both locations. There is a significant difference between the proportion of apo and holo Tf in the plasma and the CSF. The plasma recycles iron at a high speed therefore leaving more apo Tf. In the CSF the free iron requires stricter regulations occupying a higher concentration of holo Tf.

1.5 Objectives

There is increased evidence to support the identity of the toxic species in A β aggregations as prefibrillar, soluble oligomers.^{11,17,26,35,72,73} These intermediary oligomers are presumed to be formed during the *lag phase* of the hypothesized *nucleation-dependent polymerization* and may be associated with a pre-nuclear intermediate.²⁶ The focus of this research is the early aggregation of A β targeting the production of toxic intermediates. Through the manipulation conditions, the rate of A β aggregation can be controlled for the detection of the initial events involved in aggregation.

1.5.1 Plasma Inhibitory Protein

A β formation and its potential to aggregate are found throughout the body. Distinct from the actions within the brain, the body contains an inhibition mechanism to compete with the potential of A β aggregation. There are many attributes involved in A β aggregation and its inhibition. The focus within this research is the inhibition by plasma inhibitory proteins, specifically Tf a glycoprotein that is responsible for iron homeostasis throughout the body. Tf is found in significant concentration in both the plasma and CSF, but is decreased with the onset of AD, it is a viable option for further investigating this aggregation processes.

1.5.2 The Independent Action of Tf

The responsibilities of Tf for iron transportation have been the only proposed mechanism for Tf inhibition of A β aggregation. The influence of iron on A β is known to produce oxidative stress for the commencement of aggregation and upon the removal of iron early aggregation is disfavoured. This mechanism of inhibition based on the removal of iron has been demonstrated, the remaining inquiry is on the direct inhibition of Tf upon the A β aggregation.

1.5.3 A Mechanism of Inhibition

There are many naturally occurring aggregating systems that implement inhibition mechanisms for regulation. Based on known reactions, a hypothesized model of Tf inhibition on early-aggregation can be formed. With the addition of Tf to the aggregated

system of A β we are hypothesizing that Tf binds to a specific oligomeric species that is found in the early stages of A β oligomerization thus preventing the further addition of monomeric A β to continue the aggregation process.

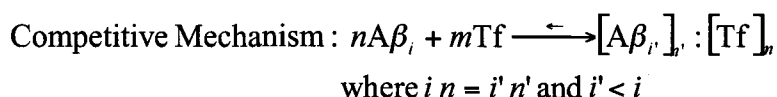


Figure 1.7 | A Hypothesized Competitive Mechanism for the Inhibition of A β aggregation by Tf | Based on the nucleated-dependent polymerization model with focus on the earlier stages of aggregation, a competitive mechanism is proposed. This mechanism entails that Tf, the inhibitor coats the A β oligomeric species preventing further monomeric additions is the predicted interactions to halt aggregation.

1.5.4 The Identification of the Oligomeric A β Species

Structural information of proteins and peptides contains a wealth of knowledge pertaining to characteristics and actions within the body. Aggregation of A β is a highly dynamic process where the instability of the intermediates formed pose difficulties to isolation. There has yet to be a defined isolation for intermediary oligomers formed during A β aggregation. Protein NMR techniques as well as CD secondary structural determination are commonly used detection techniques used for such systems. The introduction of other techniques does not provide the range of dynamic motion required for the natural pathway of aggregation.

1.6 Protein NMR

As discussed previously, in the description of A β oligomerization, difficulties arise upon the isolation of oligomeric intermediates of A β fibrils due to the dynamic exchange with the monomeric population of the peptide sample. This in turn causes complications with the detection of A β oligomers. If isolation is a problem then neither crystallographic nor other diffraction methods are viable possibilities. Additionally, A β intermediates are highly dynamic and crystallization attempts would risk altering the conformational state. The investigation of solution-state NMR is therefore an effective option for the investigation of early and dynamic stages of A β aggregation at residue/atomic resolution.

1.6.1 Nuclear Magnetic Resonance

As part of NMR detection, the sample under analysis is placed in a *static magnetic field*, \mathbf{B}_0 . Upon the introduction of a given *radio frequency (RF) pulse* (*i.e.* \mathbf{B}_1), there is an exerted torque on the net magnetization \mathbf{M} , which rotates the magnetization to the xy plane. Through the influence of \mathbf{B}_0 , the magnetization precesses at a resonance frequency or Larmor frequency ν_0 resulting in a current that is observed by the detection coil, creating recordable observations (*i.e.* the *free induction decay*, FID). The system is then returned to its thermodynamic equilibrium where the transverse \mathbf{M} will decay with time until it achieves a parallel orientation to \mathbf{B}_0 . The pulse sequence can therefore be repeated and several FID are co-added for the purpose of signal averaging. If the signal of interest arises from solutes in protonated solvents (*i.e.* H₂O) the intense solvent line must

be suppressed prior to detection to avoid limiting the dynamic range. For this purpose it is typical to use a *water gradient-tailored excitation (WaterGATE)* which allows the use of undeuterated solvents for NMR analysis.^{74,75}

The *Fourier transformed (FT)* co-added FIDs then produce the conventional frequency domain spectrum. The dominant NMR parameters that define an NMR spectrum in the frequency domain are: chemical shifts (δ), spin-spin coupling constants (J) and the line-widths. The chemical shift effects the local chemical and spatial environment of a spin, while the line-width (typically measured as full-width at half-height for a given NMR line, $\Delta\nu_{1/2}$) reports on dynamic processes that affect the transverse relaxation time (T_2), such as ps-ns interactions and chemical exchange, especially in the ms- μ s time-scale.

1.6.2 NMR Sample Requirements

Protein NMR is highly dependent upon line-broadening and relaxation rates for detection. Though NMR parameters are taken into consideration, these conditions are often contradicted with the parameters that influence peptide aggregation. The increase of aggregation (average weight of the sample) there is an increase of line broadening, decreases in relaxation rates and a lowered sensitivity is observed. To improve sensitivity, increased temperature is applied during detection to increase mobility of the sample as a whole. Alternatively, if a decreased rate of aggregation is required, a decrease of temperature is applied to prevent mobility and further aggregation.

Another sample condition implemented to improve NMR detection is the pH of the peptide sample. For NMR protein detection pH of 3 – 5 is applied. This weakly acidic media provides minimal exchange rates for the amide protons with the water present used as a solvent. Typically acetic or formic acids are utilized as buffer systems to implement a fix the pH. In addition the system requires a field frequency lock, which is applied through the addition of a deuterated substance –*i.e* deuterated water (5-10% D₂O). With the involvement protein complexities, all parameters are taken into consideration for the overall goal of improving detection.

1.6.3 A β Detection Utilizing NMR

A β in the monomeric form is highly dynamic and sufficiently short (*i.e.* < 43 amino acids) to be suitable for solution NMR. Even a simple 1D experiment provides a highly sensitive and informative representation of A β : the chemical shift indicates the presence of random coils and/or helical stretches, while the line-widths are sensitive to the presence of oligomers in exchange with the monomeric A β population. This can be appreciated by comparing 1D NMR spectra before and after filtration and/or the introduction of aggregation (Chapter 3: *Results and Discussion*, Figure 3.1.).

While 1D experiments are useful for qualitative assessments of the oligomerization status of A β , more quantitative methods are required to rigorously characterize the effect of sample condition and of oligomerization inhibitors on the A β self-association equilibria. For this purpose two main classes of NMR experiments have been used: the *saturation transfer difference* (STD) experiments⁷⁶ and the non-selective

off-resonance relaxation (ORR) experiments.⁷⁷ Both STD and ORR measurements, when implemented in-conjunction with 2D detection blocks (*i.e.* TOCSY experiments), probes oligomerization at residue resolution.^{77,78} The two quantitative, STD and ORR are complementary to each other because they affect different types of artifacts through detection. STD is predominately diffused by monomer contributions due to its initial saturation point, which also lead to partial oligomer spin-diffusion, and offset effects. ORR on the other hand is not affected by the artifacts in STD, but lacks the detection abilities for the information on glycine residues and requires the use of strong, possibly destabilizing, spin-lock fields. With the combination of STD and ORR detection, there is a more reliable and specific indication of the oligomerization status of A β .

The detection of STD-NMR was used for the weak interactions of biological macromolecules –*i.e.* small ligands.⁷⁹ The strength of the STD method is targeted specifically for the detection of weak binding of a K_d ranging between 10^{-3} to 10^{-8} M and 1 nM of receptor with high sensitivity.⁷⁹ With the recent increase in the field of protein chemistry, STD detection has been implemented for the self-recognition mapping of oligomerizing peptide matrices.^{72,73}

This change of detection by STD-NMR differs considerably from the detection of macromolecules with respect to the location and target of the selective saturation that is introduced into a tumbling system (Figure 1.8). For the involvement of STD experiments for the detection of monomer - oligomer interactions the selective RF field is saturated on the monomeric signals (*e.g.* typically methyl or aromatics). This is applied for the fact that the resonance frequencies of the oligomeric intermediated remains unknown. The

presence of an oligomeric population is identified through this applied saturation; for the transfer of this saturation can diffuse through the monomeric peptide to the added oligomeric portion, where the diffusion is more effective due to slow tumbling of the larger constituent. The saturation is then transferred back to the original monomer, which is what results in the detected of a STD signal. This difference of applying the saturation to the larger constituent improves sensitivity and establishes a well-resolved signal for detection. This variations of detection for A β monomer – oligomer exchange is accompanied by three potential sources of artifacts. These artifacts must be considered upon analysis of A β self-association before any conclusions can be drawn from the spectra: offset-effects, intra-monomer cross-relaxation, and partial intra-oligomer spin-diffusion⁷⁶.

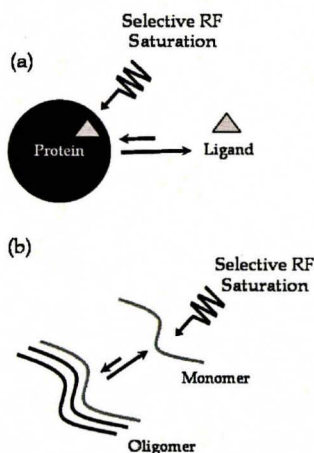


Figure 1.8 | The Mechanism of Saturation Transfer Difference Experiments | The original purpose of the STD NMR experiment was to identify the weak binding of protein to ligand (a). With the capability to identify weak interactions, the STD experiment was utilized for the detection of the monomeric to oligomeric exchange (b). This process had been proven useful for such binding through the amyloid aggregation process.

The ORR pulse sequence is based on the tilt angle of the effective field during spin lock, the static magnetic field and the repetition delay.⁷⁷ In order to measure non-selective off-resonance ^1H relaxation rates for varying conditions of amyloidogenic peptide samples, the specific probing of the early oligomer distribution at residue resolution is required. Targeting early $\text{A}\beta$ aggregation is primarily based on sample preparation methods, the changes exhibited by the peptide is detected by NMR. With sensitivity specific for detection on a residue basis the changes upon aggregation can be further examined. This will ultimately provide valuable information on the 'hot spots' within the peptide that are involved in self-recognition.^{77,78} This ORR-based method is crucial to map, at residue-resolution, self-recognition for amyloidogenic peptides and it overcomes previous experimental challenges associated with the measurement of other ^1H relaxation rates that scale linearly with $J(0)$ (*i.e.* R_2 and selective R_1).^{77,78}

Materials and Methods

Chapter 2

Materials and Methods

2.0 Materials

A β 12-28 (^+H_3N -V12HH QKLV FFAE DVG SNK28-COO $^-$) was purchased from EZBiolab in Westfield Indiana as a lyophilized powder with a minimum purity of 96.5 %. The purity and the molecular weights (*i.e.* 1.96 kDa for the 17 amino acid) were checked through HPLC and mass spectrometry by EZBiolab. Each experimental trial that involved a comparison between peptide solutions was based on the same batch of purchased peptides to avoid any bias due potential variability. Each batch was purchased in 5.0 mg or 1.0 mg pre-weighed vials that were used for sample preparation.

The partially iron-saturated Tf, apo-Tf and holo-Tf where all purchased from Sigma-Aldrich, Oakville Ontario, as lyophilized powders with > 98 % purity. All proteins were reported to have a molecular weight of 76 – 81 kDa with a solubility of 50mg/mL in H₂O. The partially saturated human serum Tf contained 300 - 600 μ g/g of iron, which corresponds to 20 – 40 % saturation with ferric irons.

2.1 Sample Preparation

2.1.1 Preparation of NMR Samples of the A β 12-28 Peptide

A 50 mM deuterated sodium acetate (d₃) buffer was prepared from a mixture of deuterated acetic acid (d₄) and sodium hydroxide used to adjust the pH to 4.7. The A β sample was stabilized under a pH of 4.7. Lower pH values from the reported

physiological value of pH 7.4⁴⁷ provided an unfavorable fibril formation equilibrium. The addition of 10 % D₂O (Cambridge Isotopes, Andover Massachusetts) was added to the acetate buffer for NMR locking purposes and filtered at 0.22 µm. The buffer was then verified for purity through 1D ¹H-WG NMR experiments, prior to its use for sample preparation. This buffer composition was used because it has been previously shown to stabilize the early Aβ₁₂₋₂₈ oligomers formed.⁴⁰

Aβ₁₂₋₂₈ was stored as a lyophilized powder at + 4°C in a dry, sealed environment. The peptide sample was treated with care for the powderized form of the peptide is highly volatile and therefore a protective mask to avoid inhalation. In addition, to minimize handling, Aβ₁₂₋₂₈ was purchased in pre-weight vials of 5 mg. The sample of Aβ₁₂₋₂₈ was then dissolved in its original vial to minimize peptide losses. The sample was left to stand on ice for 10 – 20 minutes with minimal agitation to prevent aggregation until the peptide was fully dissolved.

The uniformly dissolved sample of Aβ₁₂₋₂₈ in 50 mM NaAc-d₃, 10 % D₂O at pH 4.7 was purified to its largely monomeric form through filtration. The non-sterile Ultrafree[®] 30 kDa filter units were used to ensure minimal binding of the peptide. Each filter held a maximum of 500 µL of the Aβ₁₂₋₂₈ sample before experiencing a deficiency in filtration. An Allegra[™] 25R Centrifuge was used in conjunction with a TA-15-1.5 rotor, spun at 4,000 rpm for 5 minutes at + 4°C. Prior to sample filtration, potential residual glycerol from the filter units was removed from the filter through centrifugal washing with 50 mM deuterated (d₃) sodium acetate buffer for 5 – 7 cycles. Aβ₁₂₋₂₈ samples were spun repeatedly with stabilization every 5 minutes in ice to

minimize the heating of the sample. Upon completion of filtration, the concentration of the filtered peptide was assessed through 1D ^1H -WG NMR spectra. A series of individual A β 12-28 were prepared through filtered weighed-lyophilized powder sample at varying concentrations to be used as reference spectra to perform a quantitative measurement.

After filtration, aggregation was re-introduced in a controlled manner through the addition of salt, which shields the electrostatic interactions and promotes the intermolecular collapse of the hydrophobic core of the peptide.⁸⁰ Specifically, a varying amount of sodium chloride was added to the filtered peptide sample. Care was taken to ensure that the same amount of peptide was consistently used for all samples. The NaCl salt was added using aliquots from concentrated stock solutions (5 M and 1 M) which were added to the A β 12-28 sample. Addition from different stock solutions was performed to minimize volumetric errors. All volumes added to the peptide sample were in the 1 μL to 15 μL range, reducing the dilution factor to a negligible < 4%.

2.1.2 Protein Sample Preparation

The partially saturated Tf, apo-Tf and holo-Tf were obtained as a lyophilized powder from Sigma-Aldrich, Oakville Ontario and refrigerated at + 4°C in a sealed, dry environment. 500 μM samples of each protein were prepared by dissolving a weighted amount of the powder in 50 mM deuterated (d_3) sodium acetate buffer, pH 4.7 with 90/10 doubly distilled H_2O to D_2O . The buffer batch was consistently used for all peptide and protein preparations involved in our comparative analyses. After dissolving the

protein in the acetate buffer, the solution was kept on ice and/or refrigerated at + 4°C. The protein concentration was verified through the QuantiPro™ BCA Assay Kit from Sigma-Aldrich Oakville, Ontario. Bicinchoninic acid (BCA) is a sensitive and reliable procedure for determining protein concentrations. The procedure utilizes alkaline reduction of Cu^{2+} to Cu^{1+} by proteins in addition to the formation of a bicinchoninic acid/ Cu^{1+} complex with an absorbance maximum at 562 nm. The BCA assay kit includes reagent A; an aqueous solution of 1% sodium bicarbonate (Na_2BCA), 2 % sodium carbonate ($\text{Na}_2\text{CO}_3 \cdot \text{H}_2\text{O}$), 0.16% Na_2 tartrate in 0.4% NaOH and 0.95% NaHCO_3 (BCA detecting reagent), reagent B containing 4% curpric sulfate ($\text{CuSO}_4 \cdot 5\text{H}_2\text{O}$) and a standard of 2 mg/ml bovine serum albumin (BSA) in 0.9% saline and 0.05% sodium azide (NaN_3). The reagents are mixed together in a 50:1 ratio and the BSA is used as a calibration standard. Once the reagents, standard and protein were mixed, the solutions were put in a 37 °C water bath for 30 minutes. The *optical density* (OD) measurements were obtained on a Hewlett Packard 8453 UV-vis spectrometer set at a detection wavelength of 562 nm to determine the protein concentration. The original protein samples were stored at + 4°C before and after sample preparation. Introduction of salt to the peptide sample was also applied with each volumetric addition measured from a common stock solution so that only a minimal dilution occurred in avoidance of a bias in sample comparisons. Typically the total protein solution volume added was within the range of 1 μL to 8 μL that entails a dilution effect of less than 2% for the original peptide sample.

In addition to the BCS assay, the protein concentration was also verified through the calculation of its extinction coefficient. The sequence of the prepared Tf was obtained from the protein database (**PDB**).⁵⁸ Through the use of the University of Illinois's web-based Biological WorkBench version 3.2,⁸¹ an extinction coefficient was calculated in $M^{-1}cm^{-1}$. based on Gill and von Hippel's Analytical Biochemistry paper in 1989.⁸² With this information the concentration was determined through Beer-Lambert's Law of an absorbance at 280 nm.

$$A = \epsilon bc$$

This equations outlines that the absorbance (**A**) is proportional to the extinction coefficient (ϵ) $M^{-1}cm^{-1}$, the path (**b**) length of the cuvette (0.5 cm), as well as the concentration of the sample (**c**) in M. Three absorbance were obtained averaging out the value along with the obtained concentration resulting from the BCA assay

2.2 Methods

2.2.1 NMR Spectroscopy

NMR data was collected at 293 K using either a Bruker Avance 600 MHz NMR spectrometer with 5 mm *inverse triple resonance multinuclear (TBI-Z)* probe or Bruker Avance 700 MHz NMR with *inverse triple resonance (TCI-Z)* cryoprobe located within the NMR facility of McMaster University. Both NMR magnets employed XWINNMR for the management of NMR experimental acquisition and processing.

1D 1H NMR experiments are highly useful and highly sensitive NMR techniques that can be utilized for every NMR sample. Each peptide, protein and buffer samples

prepared was checked and monitored through the acquisition of 1D ^1H NMR spectra. All spectra acquired were recorded with 128 scans, 32 dummy scans and a spectral width of 8389.26 Hz sampled with 4096 complex points and a repetition delay of 1 s. The *Watergate* water suppression by gradient-tailored excitation was applied to all pulse sequences used throughout the analysis. (Figure 2.2) It is an excellent tool to use for the suppression of solvents, specifically water. The water suppression was achieved by the addition of a binomial 3-9-19⁷⁵ *Watergate* gradient spin-echo (WG) to remove the water signal before acquisition. The purpose of the 3-9-19 pulse train is to ensure that the net rotation of the H_2O magnetization is relatively close to zero while the remaining portion of the spectrum was flipped 180° therefore acquiring a spectrum of predominately the analyte peptide without limiting the dynamic range with an intense residual water peak. This permits the minimal uses of deuterated solvents such as 10% D_2O to satisfy both the spectroscopic and biological requirements. WG has been incorporated in both 1D and 2D pulse sequences utilized in all NMR experiments in this investigation.⁷⁴

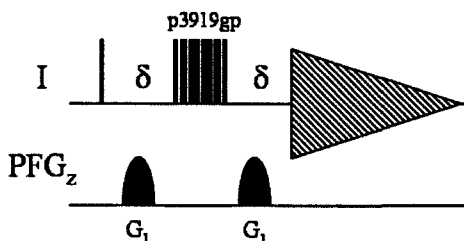


Figure 2.1 | 1D ^1H -WG NMR Pulse Sequence | Watergate is a technique for solvent suppression achieved through the addition of a 3-9-19 pulse train. PFG is the pulsed field gradient in the z-direction providing a better detection as well as δ delay. This was implemented for sequences used in both the AV 600 MHz and the 700 MHz Bruker NMR systems.

2.2.2 1D Saturation Transfer Difference (STD) Experiments

Saturation transfer difference (STD) experiments have been widely used in the past to screen for small ligand interactions with biological macromolecules, namely proteins and nucleic acids.⁷⁹ With the capability of probing weak interactions with great sensitivity STD experiments were recently tailored for mapping the self-recognition in oligomerizing peptide systems.^{76,83} This novel approach for the utilization of the STD pulse sequence has switched its target from drug rationalization to monomer-oligomer interactions. 1D-STD experiments were used here to monitor the effect of Tf on the aggregated A β 12-28 samples.

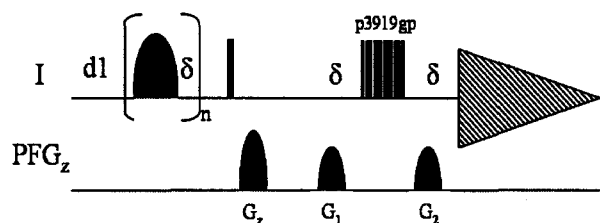


Figure 2.2 | 1D ^1H -STD NMR Pulse Sequence | A methyl peak is saturated through a continuous pulse. A PFG is pulsed field gradient in the z-direction allowing analytically accurate, automated adjustments of shims and dl is relaxation delay. An implementation of WaterGATE for water suppression was also used. The STD was used for both AV 600 MHz Bruker NMR with an TBI-Z probe and the 700 MHz NMR with a TCI-Z cryoprobe at 293 K.

STD experimentation is based on the difference between on and off resonance spectra. In order to achieve on-resonance saturation, the carrier frequency of a Gaussian pulse train is applied to a methyl on the monomeric A β state (typically 0 to -1 ppm)⁷⁶. (Figure 2.3⁷⁹) Specifically this magnetization was applied to the valine methyl group within the hydrophobic core region of A β at approximately 0.75 ppm. Off-resonance

saturation or *saturation transfer reference* (STR) was obtained by saturating at 30 ppm, a region in which no specific ^1H saturation would occur (typically 25 to 50 ppm).⁷⁶ The saturation transfer difference spectra were obtained by subtracting on-resonance and off-resonance spectra through phase cycling.

For a filtered, largely monomeric, A β 12-28 sample the magnetization applied to the methyl group then propagates through the monomer via a network of intramolecular ^1H - ^1H cross-relaxation pathways. Upon the existence of a high contribution of monomers within the sample the magnetization pathways would solely consist of spin diffusion through the monomeric target. In the case of an aggregated sample with the presence of a monomer-oligomer exchange, the magnetization is transferred from the originally targeted monomeric state to the oligomeric state. With the subtraction of the STD from the STR spectra, the resulting amino acid peaks that are engaged in the exchange produce a peak in the final STD spectrum.

Selective saturation was achieved using a train of 40 Gaussian-shaped pulses of 50 ms each, separated by a 1 ms inter pulse delay, resulting in total saturation time of ~2 seconds which was preceded by a 100 ms inter-scan delay. The strength of each saturating Gaussian pulse was 110.23 Hz with a 1 % truncation and 1000 digitization points. A 30 ms spin lock pulse with strength of 2.5 kHz was applied to suppress the residual protein signal in all STD and saturation transfer reference (STR) experiments. For the STD experiment 128 scans and 8 dummy scans were acquired, which were reduced to 32 scans and 32 dummy scans for the more sensitive STR spectra. For each titration point two STR and four STD replica spectra were collected. All STD and STR

replicas were then added to increase the S/N ratios. The 6.88-7.25 ppm spectral region was used to determine the STD/STR ratios and the related errors were evaluated using the standard deviation of the individual replicas and error propagation. Before data acquisition for each protein titration point, STD experiments were performed on a filtered A β 12-28 sample as well as on an aggregated A β 12-28 sample without protein to confirm sample stability.

2.2.3 2D Off-Resonance Relaxation (ORR) Experiment

The measurement of ^1H off-resonance nonselective relaxation rates ($R_{35.5^\circ, \text{ns}}$) has been recently proposed as an effective method to probe peptide self-recognition, opening new perspectives in the understanding of the pre-fibrillar oligomerization processes in amyloidogenesis. The nonselective off-resonance ^1H relaxation NMR pulse sequence is derived from the well-established 2D-TOCSY experiment by inserting an adiabatic spin-lock between the interscan delay and the first 90° pulse of the 2D detection block.⁷⁷ All ORR experiments were acquired at 700 MHz with an off-resonance trapezoidal spin-lock including two adiabatic pulses of 4 ms duration and applied at the angle of 35.5° to ensure optimal NOE/ROE compensation in the spin-diffusion limit.^{77,83} The total spin-lock durations were 13 and 88 ms.^{77,83} Strength of the off-resonance and TOCSY spin lock was 8.25 and 10 kHz, respectively. The interscan delay between the end of the acquisition and the start of the first adiabatic pulse was 2 s. The spectral widths for both dimensions were 8389.26 Hz with 256 t_1 and 1024 t_2 complex points, respectively. Water suppression was achieved using the binomial 3-9-19 Watergate gradient spin-echo

(WG).⁷⁷ For each experiment, 16 scans and 128 dummy scans were employed. For the 13 ms spin-lock time that resulted in intense signals so only one data set was obtained, while at 88 ms

Two replicas were collected. All 2-D replica sets were co-added to increase the S/N ratios and processed with Xwinmr (Bruker, Inc.) using a 90° phase shifted squared sine bell window function for both dimensions prior to zero filling. The 2D cross-peak intensities were measured with Sparky 3.111⁸⁴ by Gaussian line fitting using the fit peak heights. The standard deviation of the differences in fit heights between two copies was used to estimate the error of the individual spectra. The error of the sum was scaled up proportionally to the square root of the total number of scans. For all residues, the H_{α,i}-H_{N,i} cross-peaks were used for data analysis, with the exception of G25 and of the N-terminal V12. G25 was omitted from the analysis due to the overlap of its degenerate H_α protons, while for V12, the H_{α,12}-H_{Me,12} cross-peak was used to probe H_α relaxation rates. The nonselective off-resonance relaxation rates in s⁻¹ were computed from the experimental fit heights though the equation:⁷⁷

$$I(t) = I(t_0)e^{-R(t-t_0)}$$

$$R_{35.5^\circ,ns} = \ln(\text{fit height at 88 ms} / \text{fit height at 13 ms}) / (0.088s - 0.013s)$$

Where I is the intensity of the ORR contour at time t and initial time (t₀). R_{35.5°,ns} is the nonselective relaxation taken at title angle 35.5°. The nonselective off-resonance relaxation rates calculated based on the equation above are within error of the off-resonance relaxation rates calculated using five different spin-lock times. The measured

rates and the related errors were then normalized with respect to the maximum observed rate.

2.2.4 Transfer 2D Nuclear Overhauser Enhancement Spectroscopy (Transfer 2D-NOESY) Experiments.

2D-NOESY experiments are designed to effectively measure ^1H - ^1H *nuclear Overhauser effects* (NOEs), which result from the dipolar interactions of proton spins. In the slow tumbling time-scale, the intensity of the identified NOEs is proportional to the inverse of the sixth power of the distance between protons and therefore the NOEs are an effective probe of proton pairs within a distance of $< \sim 5$ Å. The 2D-NOESY acquisition parameters were set up as follows; 256 t_1 and 1024 t_2 complex points covering a spectral width of 8389.26 Hz in both dimensions, a repetition delay of 1.2 s, a mixing period of 100 ms, 64 scans per serial file and 128 dummy scans.

2D-NOESY data was processed through Xwinnmr (Bruker, Inc.) in a similar procedure at the 2D-ORR data collected, using a 90° phase shifted squared sine bell window function for both dimensions prior to zero filling. The 2D NOEs were identified through Sparky 3.111⁸⁴ by reference to previously assigned peaks.⁸³ There was no error calculated for the NOE data for it was a measure of NOE distances and concluded with qualitative results.

2.2.5 Inductively Coupled Plasma Experiments

Inductively coupled plasma (ICP), mass spectrometer (MS) is an analytical technique used for the detection of trace metals in environmental samples. The ultimate goal of ICP is to get elements to emit characteristic wavelengths of light which can be measured quantitatively. An ICP system utilizes nebulization to convert liquid samples into an aerosol and volatilization to remove all water from the sample leaving the remaining sample to be converted into a gas. The sample is then introduced to a plasma flame in the presence of an inert chemical environment, typically argon gas. This atomizes the sample, further breaking the gas phase bonds. At this point, the atoms within the sample gain energy for collision and emit light of a characteristic wavelength. A grating dispersion of light then quantitatively measures the sample.

A doubly distilled H₂O sample of 100 mL that was used for sample preparation was treated with 1% nitric acid (HNO₃). Detection was carried out by Kevin Ferguson BSc, the Quality Assurance Manager at the Occupational and Environmental Health Laboratory, a fully accredited *American Industrial Hygiene Association (AIHA)* laboratory in the Department of Chemistry at McMaster University. The instrument used was a Perkin Elmer, model ELAN 6100 ICP-MS following the NIOSH 7300, the standard operating procedure for analysis of solution-based iron contamination.

2.2.6 Circular Dichroism (CD) Spectroscopy

CD spectroscopy is a very sensitive method for the detection of polypeptide and protein secondary structure. This determination of secondary structure is based on the

difference between right and left circularly polarized light of a substance, for the absorption of peptide bonds in the far UV region. CD is measured in mean residue molar ellipticity with units of degree·cm²/dmol.⁸⁵

A β samples at a variety of levels of aggregation and protein concentrations were tested using CD spectroscopy. Aliquots of 250 μ L of a given A β sample were carefully transferred into a 0.1 cm path-length quartz cell and analyzed three times. Prior to sample introduction the cell was washed with a strong acid (three thorough washes) followed by three washes with distilled H₂O and six washes with 50 mM deuterated (d₃) sodium acetate buffer, pH 4.7 with 90/10 doubly distilled H₂O to D₂O, to ensure consistency with the conditions used in our NMR experiments. The CD measurements were performed on a far-UV AVIV Circular dichroism (Model 410) spectrometer. Once the data was collected, the 400 μ L sample was returned to its original 500 μ L NMR sample.

All spectra were obtained at 298 K at a wavelength range of 180 - 270 nm. Measurements at lower wavelengths could not be processed due to the addition of salt for the promotion of aggregation that caused an excessive dynode voltage rise during acquisition. Control experiments of the filtered A β sample were taken as a control. Raw CD data was blank subtracted through the CD spectra that were obtained for the 50 mM deuterated (d₃) sodium acetate buffer, pH 4.7 with 90/10 doubly distilled H₂O to D₂O. Upon the addition of Tf to the peptide sample, the raw data of the control spectra of buffer plus Tf was subtracted. CD data was analyzed by CDPro, a CD interpretation software containing SELCON3, CDSSTR and CONTINLL. These three analysis

programs that compare experimental data with a database of known protein structures. The deviation of the data is based on the *root mean squared deviation* (**RMSD**) and the *normalized RMS deviation* (**NRMS**) values between the calculated and experimental spectra.

Results and Discussion

Chapter 3

Results and Discussion

3.0 Sample Preparation for the Focus of Early A β Aggregation

3.0.1 The Control and Stabilization of the A β 12-28 Peptide Sample

The two most abundant A β lengths produced *in vivo* are A β 40 and A β 42. The analysis of oligomerization of these two A β species has been difficult due to the rapid rate of aggregation as well as the change of state that is involved as a result of aggregation (*i.e.* the distribution of soluble oligomer and insoluble fibrils).

Since hydrophobicity is a major determinate for aggregation, it can be used to experimentally control A β aggregation. This study used A β 12-28 that contained the CHC region, but lacked the C-terminal hydrophobic region contained in the full-length peptide, resulting in a decreased the rate of aggregation and the stabilization of the early oligomeric aggregates.^{47,83}

The 1D ¹H-WG NMR spectrum of the filtered 650 μ M A β 12-28 was analyzed based on the line-width. (Figure 3.1) Due to the decrease in size of the fragment, the fast tumbling rate of the monomeric peptide was represented by sharp, intense NMR peaks. Through the addition of salt to the filtered A β 12-28 sample, aggregation occurs. The large oligomers produced do not have a distinct chemical shift and become too large for detection by solution-NMR. With the increased MW, there is a decrease in tumbling rate within the solution producing broadened peaks. This entails that the oligomeric portion of the sample exhibits an exchange process (K_d range μ M – mM) with the pre-existing

monomeric A β resulting in broadening peaks in comparison to the original monomeric sample.

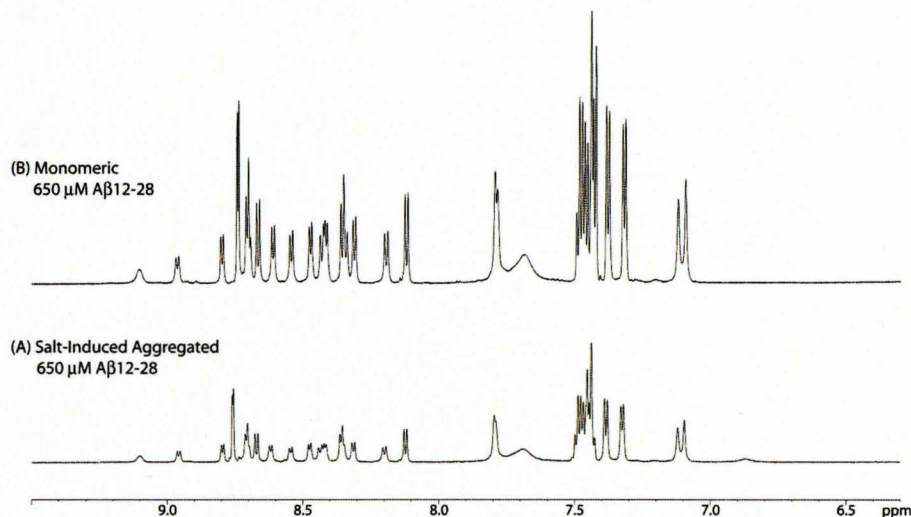


Figure 3.1 | 1D ^1H -WG Spectral Detection of the Aggregation of A β 12-28 | 650 μM of A β 12-28 is the targeted peptide representing the full-length A β fibril formation peptide. (B). The monomeric form of A β 12-28 produces well defined peaks. (A) The addition of aggregation to the peptide results in significant peak broadening. Both samples were prepared at 650 μM in 50 mM of deuterated sodium acetate buffer with 10% D $_2$ O and filtered at a 30 kDa cutoff. The NMR data was collected on a 700 MHz Bruker NMR with TCI-Z cryoprobe at 293 K. Monomeric A β was tested within 24-hrs after filtration, while a 30-day stabilization period was implemented for the detection of aggregated samples.

3.0.2 Effectiveness of Filtration

Another way of reducing aggregation is through the removal of the ‘seed’, otherwise known as the *critical nucleus*. The *critical nucleus* is the intermediate oligomer that as described in *nucleated polymerization*, controls the rate and progression of aggregation.⁵¹ The sample of A β 12-28 is obtained as a lyophilized powder and is dissolved into a 50 mM NaAc-d $_3$ buffer, with 10% D $_2$ O. The resultant sample is highly unlikely to be in the pure monomeric state due the high local concentration of the peptide

that occurs during dissolution process and favours the formation of oligomers. With the possibilities of oligomer formation, filtration is utilized which relies on in the physical removal of the A β intermediates. The remaining A β monomers are highly stable and will remain in the monomeric state for an extended period due to the lack of a *critical nucleus* present to initiate oligomerization. Unfortunately the process of filtration may be accompanied by a ‘cake affect’, additional build up of oligomers on the surface of the filter. (Figure 3.2) Batch-dependent results are highly apparent for the peptide samples, therefore the preparation of a common filtered stock solution is required.

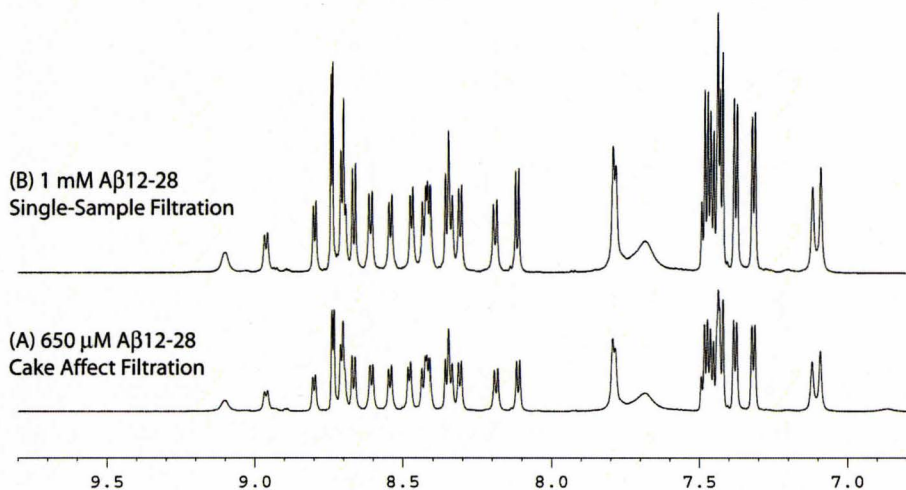


Figure 3.2 | The Observation of ‘Cake Effect’ Through Filtration of A β Peptide Samples | Upon the treatment of filtration on a 1 mM A β 12-28 of a large batch size has great potential to experience a cake effect on the surface of the filter. (B) 1 mM of A β 12-28 was prepared on a single sample basis. (A) 650 μ M of A β 12-28 originally started off as 1 mM A β 12-28, but with a large sample size, almost 35% of the peptide concentration was lost. The NMR data was collected on a 700 MHz Bruker NMR with TCI-Z cryoprobe at 293 K. Monomeric A β was tested within 24-hrs after filtration, while a 30-day stabilization period was implemented for the detection of aggregated samples.

3.0.3 Influence of Salt on the Aggregation of A β 12-28 peptide

Once the monomeric A β 12-28 has been established, a stable, reproducible and manageable method of aggregation is required. As commonly known the addition of salt promotes peptide aggregation through shielding the electrostatic interactions within A β allowing the exposure of the hydrophobic region of the peptide.^{72,80,7}

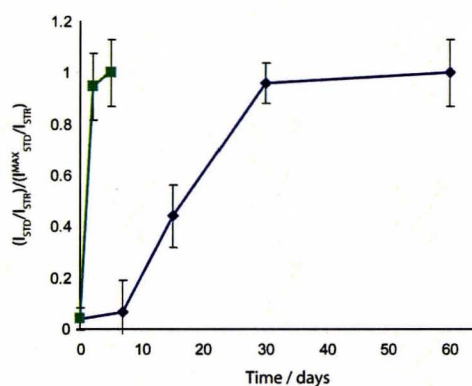


Figure 3.3 | The Stabilization Periods Associated with the Addition of Salt to the A β Peptide Sample | The addition of 40 mM of salt to 650 μ M of A β 12-28 with from stock solutions; 1 M (■) and 5 M (◆) were tested for stabilization. The time line that the samples were tested was at 0 - 60 days. All values were measured through 1D 1 H-STD NMR experiments with a 700 MHz NMR with a TCI-Z cryoprobe at 293K.

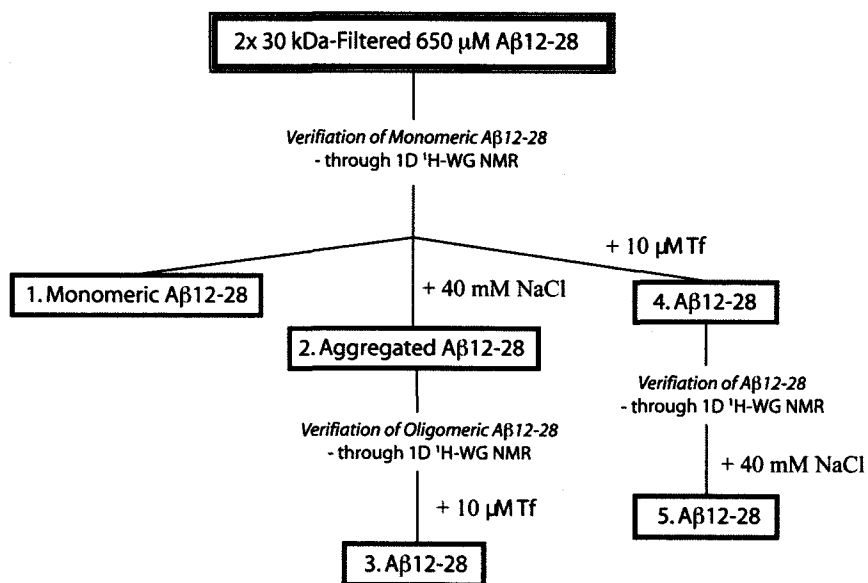
NaCl was added to A β 12-28 samples at various concentrations ranging from 0 mM to 40 mM and monitored by 1D STD. (Figure 3.3) Measurements for an individual samples were repeated over a 60-day period to ensure final sample stability. The goal of this experiment was to determine the stabilization period required for salt-induced aggregation. Upon the addition of small volume of a 5 M stock solution of salt, to minimize dilution affects, the stabilization period was found to be within a 30-day period. The addition of salt was also introduced through a 1 M stock solution that required larger volumes added, but resulted in shortened stabilization period of 2 days.

3.1 Verification of Tf's Involvement with the A β 12-28 Peptide Sample

3.1.1 *The ability of Tf to Disrupt the Dynamic Exchange between Monomeric and Oligomeric States of A β 12-28*

It has been demonstrated that Tf possesses an inhibiting affect on A β oligomerization *in vitro* with regards to the segment of A β 25-35.⁸⁶ These results were obtained through the analysis of Congo red dye binding to A β -fibrils in the presence of Tf. The objective of this investigation is to gain a greater insight on the interactions of Tf and the peptide, focusing on the A β 12-28 segment through protein NMR detection techniques.

To verify the interactions between Tf and A β , the following samples were prepared as outlined in Chapter 2: *Material and Methods*. Three common samples are familiar throughout the various experiments performed in this investigation. A pre-treatment filtration procedure that physically removed oligomeric A β from the sample results in the first reference sample representing a high A β monomeric contribution. The filtered sample is the reference sample for which an aggregated sample of A β is formed through the addition of 40 mM NaCl. The effects of the addition of Tf before and after the onset of aggregation to the A β samples were investigated. (Scheme I)



Scheme I: Verification of the Interaction of Tf and the Amyloid- β Peptide through 1D ^1H -WG NMR

The 1D ^1H -WG NMR spectrum of the filtered, 650 μM sample of A β 12-28 was used resulting in low relaxation rates that contribute to sharp, intense peaks within the spectrum. (Figure 3.4/A) In contrast the aggregated A β 12-28 sample, (Figure 3.4/B) containing a distribution of varying MW oligomers had a slow tumbling rate resulting in the longer relaxation as indicated by broadened, less intense peaks. The aggregation inhibitory abilities were tested through the addition of 10 μM of Tf before and after the aggregation of the A β sample (Figure 3.4/C and D). Immediate changes occurred within the spectrum obtained to resemble a filtered, monomeric A β 12-28 sample (Figure 3.4/A). This means that the added Tf within the sample has caused an interruption of the monomer - oligomer dynamic exchange.

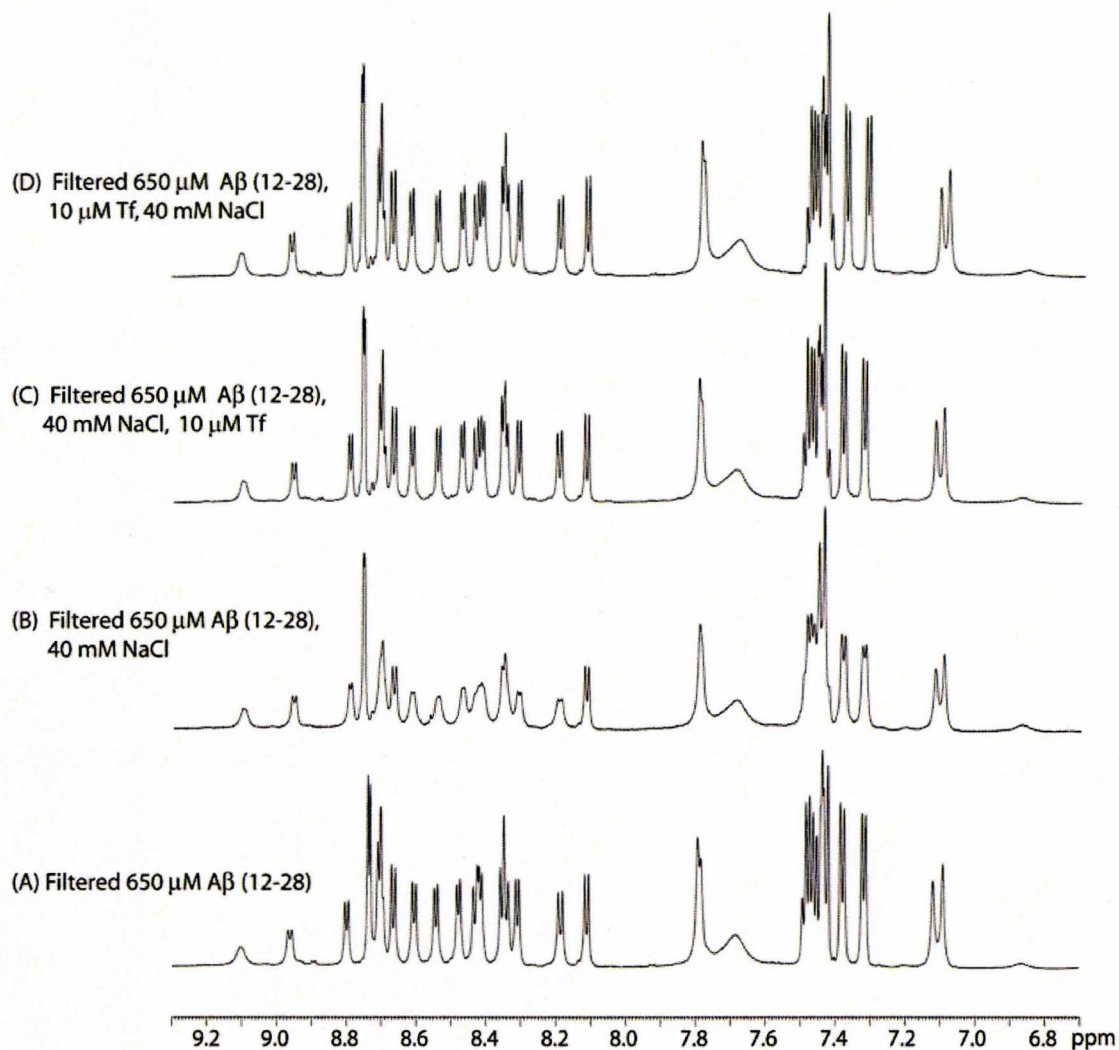
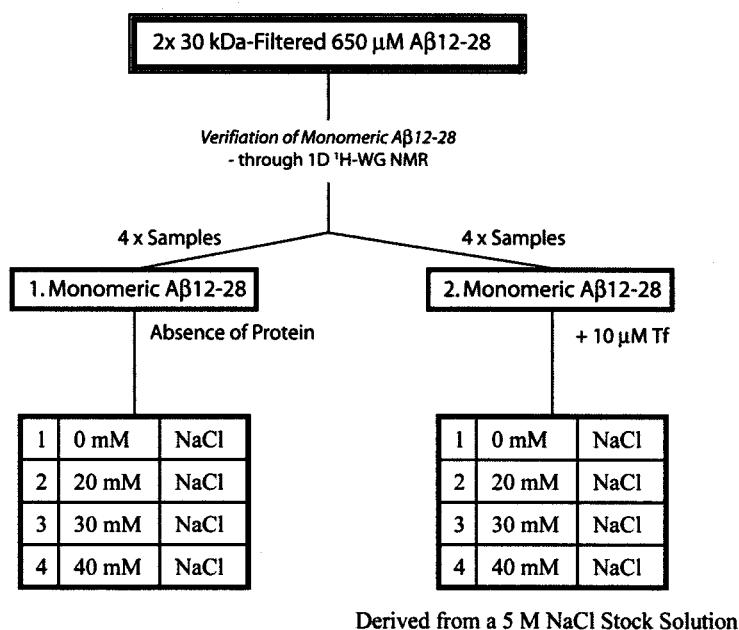


Figure 3.4 | 1D ^1H -WG Spectral Comparison of Interactions of Tf with the A β 12-28 Peptide | Changes upon the addition of Tf to salt-induced aggregated A β 12-28 were analyzed according to the line-width of the 1D ^1H -WG spectra targeting the H_α - H_N fingerprint regions. (A) Spectra of 650 μM of A β 12-28 filtered at 30 kDa representing monomeric state of A β . (B) Aggregation upon the addition of 40 mM of NaCl to the filtered 650 μM of A β 12-28 sample. (C) Addition of 10 μM Tf to the aggregated sample of (B), showing sharpened peaks as in the filtered sample in spectrum A. (D) Addition of Tf prior to the induction of NaCl also showed the same inhibition affects. All A β 12-28 samples were prepared in 50 mM of deuterated sodium acetate buffer with 10% D_2O and filtered at a 30 kDa cutoff. The NMR data was collected on a 700 MHz Bruker NMR with TCI-Z cryoprobe at 293 K. Monomeric A β was tested within 24-hrs after filtration, while a 30-day stabilization period was implemented for the detection of aggregated samples.

3.1.2 The Distribution of A β Aggregation with Respect to Pre-Nuclear A β Oligomers in the Presence of Tf

One major concern during the detection of A β interactions is the presence of different oligomeric distributions. A β 12-28 was used since it stabilizes early oligomers with the addition of varying concentrations of salt to mimic a range of aggregates formed during the early stages of oligomerization as it has been shown that with the increase of salt content within the peptide sample there is an associated increase in the oligomeric concentration.⁷²



Scheme II: Salt Titration to Mimic the Aggregation Process of A β

A new scheme is employed for peptide analysis of the varying degree of salt-induced aggregation. The pre-treatment filtration for the peptide sample was used consistently as discussed within Chapter 2: *Material and Methods*. Scheme II outlines the history of each sample, specifying the two series of the four-peptide sample sets. The two

series differ in the addition of 10 μM of Tf, after which both series are exposed to a salt gradient.

To quantify the degree of aggregation formed by these conditions, 1D ^1H -STD NMR experiments were used. The filtered A β 12-28 sample, devoid of aggregates (Figure 3.4/A) was used as a control and starting point throughout the salt addition experiments. Results were quantified using the normalized ratio of STD and STR intensities (Figure 3.5). A steady increase in STD/STR ration is observed within the filtered sample upon salt addition, noting a major jump between 20 mM NaCl and 30 mM NaCl. A consistent resistance to A β aggregation is observed in the presence of Tf. This titration was performed in replicates using either 5 M or 1 M stock solution of salt and results obtained were consistent.

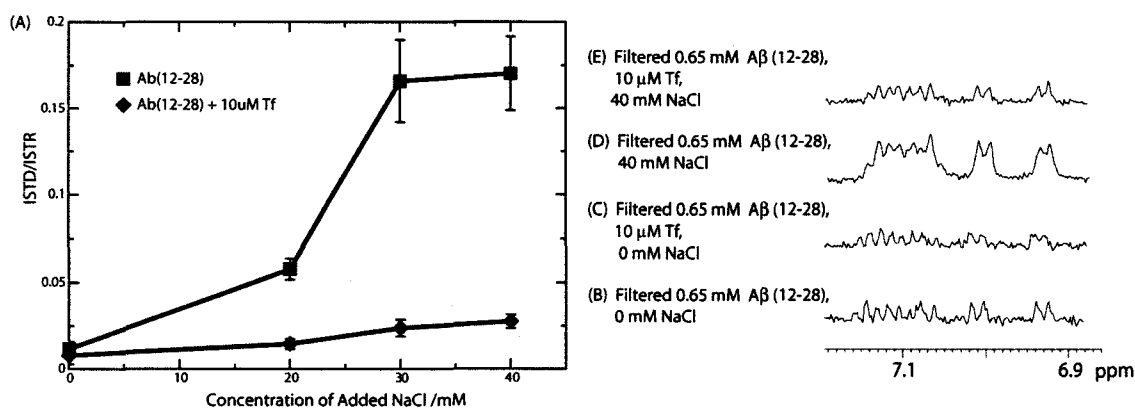


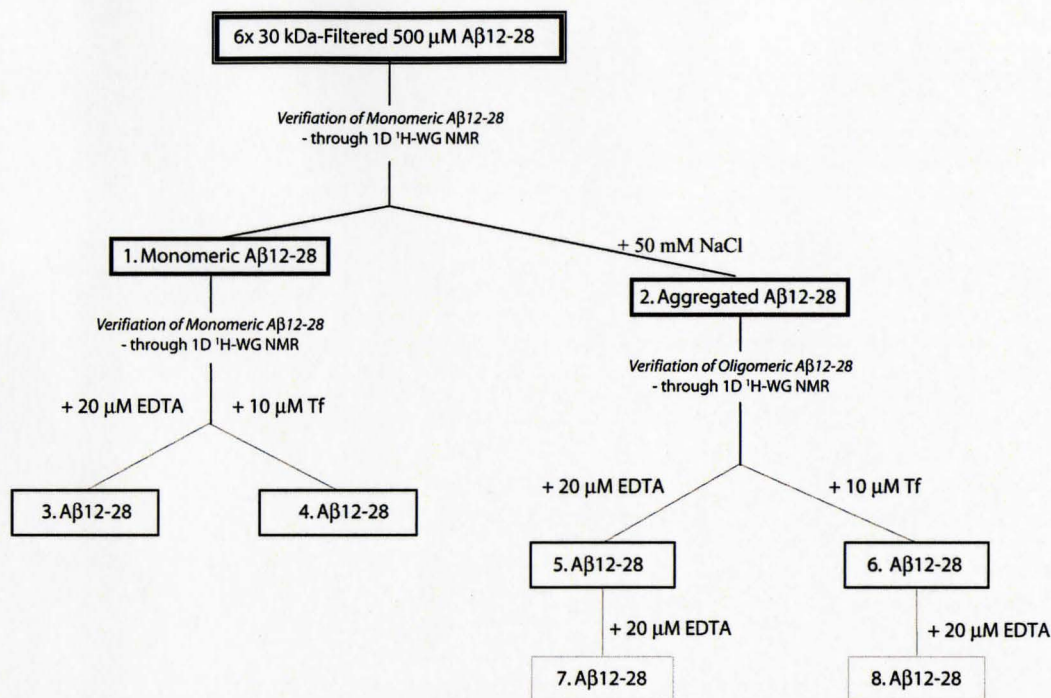
Figure 3.5 | The Effects of Progressive Aggregation on A β with the Involvement of Tf | The introduction of varying salt concentrations to a filtered/monomeric A β 12-28 sample represented an aggregation gradient. Upon each salt addition a 30-day stabilization period was respected. The graph (A) shows the intensity ratio of $(I_{\text{STD}}/I_{\text{STR}})/(I_{\text{STD}}^{\text{MAX}}/I_{\text{STR}})$ for a filtered, 650 μM A β 12-28 sample (■), with the addition of 10 μM of Tf (◆). Noting that an increase of $(I_{\text{STD}}/I_{\text{STR}})/(I_{\text{STD}}^{\text{MAX}}/I_{\text{STR}})$ relates to an increase of aggregation. The filtered sample increases proportionately to the addition of NaCl however with Tf the detectable aggregation remains unchanged. 1D STD spectra B – E reflects the raw 1D STD spectra of the initial and final point of the $(I_{\text{STD}}/I_{\text{STR}})/(I_{\text{STD}}^{\text{MAX}}/I_{\text{STR}})$ plot.

Both qualitative and quantitative NMR data were collected to test the involvement of Tf within the aggregated system. The disruption of the monomer – oligomer exchange, is apparent through the data collected; nevertheless the mechanism driving this interaction still remains unknown. Looking at the 1D ^1H -WG NMR spectrum it appears that the addition of Tf completely restores the monomeric population of the sample, producing a spectrum that greatly resembles that of the filtered – monomeric sample (Figure 3.4). STD monitored salt gradient analysis indicates that in the presence of Tf, A β resisted aggregation.

3.2 The Involvement of Iron and Tf in the Inhibition of A β 12-28 Aggregation

3.2.1 The Inhibition of A β Aggregation by Tf Not Iron Mediation

The inhibitory abilities of Tf on A β aggregation have been previously recognized to occur through the sequestration of ferric iron within the sample, which would otherwise promote A β oligomerization.⁸⁶ Indeed decreased levels of Tf and the elevated levels of iron are found within the region of senile plaques.⁸⁷ Therefore the ability of Tf to remove iron is a possible mechanism that inhibits A β aggregation.



Scheme III The Comparison between Inhibitory Mechanisms of EDTA and Tf for Aβ Oligomerization

In order to test if an iron mediated mechanism accounts for the observations seen, EDTA was added as a competitive iron chelator to Tf. The preparation of a filtered Aβ monomeric sample and a salt-induced aggregated Aβ sample are used as a comparison for the varying degree of aggregation through 1D ¹H-STD NMR experiments (Figure 3.6, Scheme II). The effect of iron removal is tested through the addition of EDTA to both references Aβ samples, showing no significant changes to the degree of aggregation of either samples. The stoichiometric metal binding for EDTA is half of that for Tf, therefore stoichiometric surplus of EDTA was added to the aggregated Aβ sample, confirming the previous results. Various conditions were tested and; results indicate that Tf is employing a mechanism of inhibition that is distinct from iron sequestration.

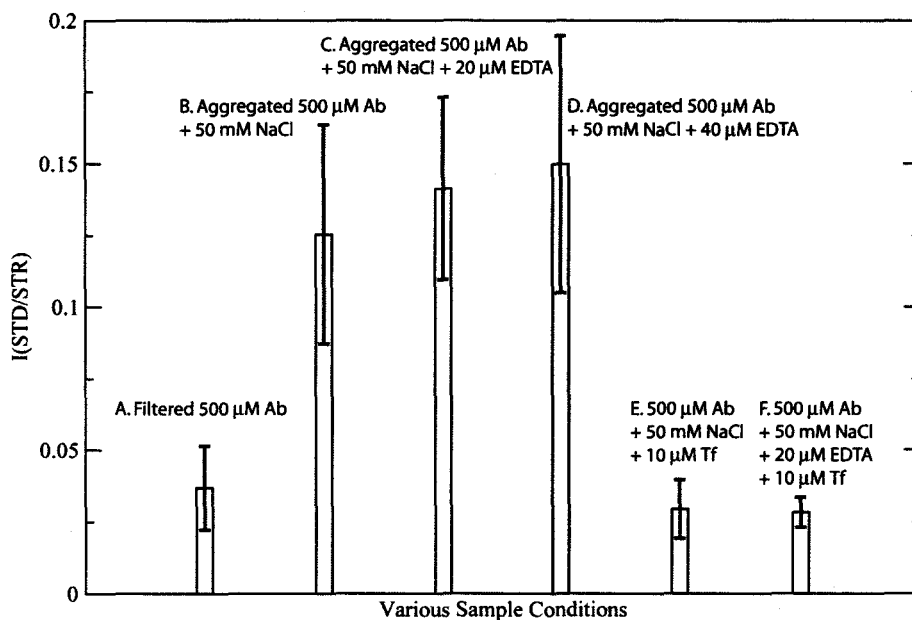


Figure 3.6 | The Sequestration of Iron and its Implications for the Tf Inhibitory Mechanism | The 1D STD NMR experiments is used to determine the degree of aggregation. The plot pertains to the intensity differences of STD and STR, in which various sample conditions were tested. (A) Filtered 500 μM A β sample. (B) The addition of 50 mM NaCl to 500 μM A β sample. (C) Aggregated sample (50 mM NaCl) with the addition of 20 μM EDTA. (D) Aggregated sample with 40 μM of EDTA. (E) Aggregated 500 μM A β sample with the addition of 10 μM Tf. (F) Aggregated sample with 20 μM EDTA and 10 μM Tf. In all cases the only decline of aggregation occurs with physical filtration or the addition of Tf. All data was collected on 700 MHz Bruker NMR with TCI-Z cryoprobe at 293 K.

3.2.2 Each Degree of Iron Saturation of Tf possesses Inhibitory ability on the Aggregation of A β 12-28.

Upon metal-binding Tf undergoes significant conformational changes that may affect A β inhibition. Tf used thus far was partially saturated with iron (20 % - 40% holo-state), which is representative of the saturation content within the plasma. After obtaining holo-Tf and apo-Tf, interactions with an aggregated sample of A β were tested through

protein titrations monitored through STD experiments, $(I_{STD}/I_{STR})/(I_{STD}^{MAX}/I_{STR})$ (Figure 3.7).

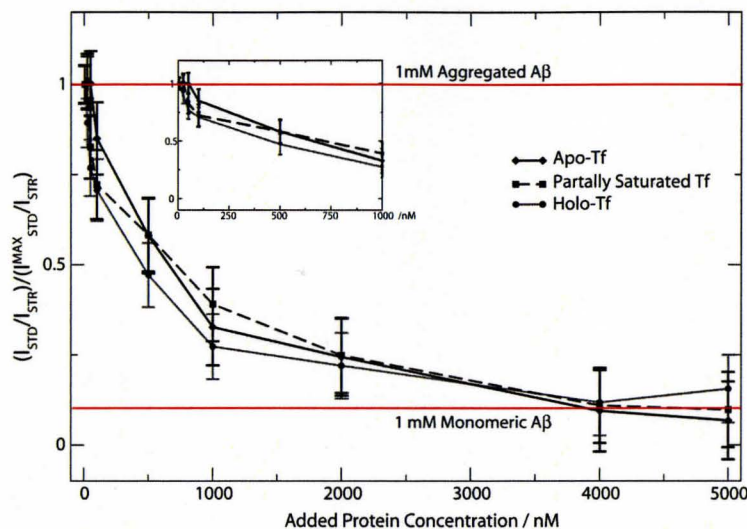


Figure 3.7 | The Various Degrees of Iron Saturation for Tf and Their Potency for the Inhibition of the A β 12-28 Peptide | The degree of aggregation was measured by $(I_{STD}/I_{STR})/(I_{STD}^{MAX}/I_{STR})$ against the Tf concentration. Apo-Tf (\blacklozenge), holo-Tf (\bullet) and partially saturated Tf (\blacksquare) were all tested. Tf at various states had a similar influence on the aggregated sample of A β . Each sample was treated with the same time delays and stabilization periods. The 1D STD experiments were carried out on an AV 600 MHz Bruker NMR with a TBI-Z probe at 293 K.

Outline of experimental setup is further discussed in section 3.3.1. The mechanism of Tf conformational change during metal-binding has not been fully described, but is commonly thought to be influenced by pH fluctuation.^{65,66} Each sample was prepared as outlined in Chapter 2, at pH of 4.7. This acidic pH is reported to slightly increase the K_d values of Tf for iron.^{65,66} The aggregated A β samples were used for the protein titrations after stabilization was achieved. The A β samples were prepared at 1 mM and were observed to show a similar inhibition potency in the presences of the various states of Tf entailing that the degree of saturation by iron does not affect the A β

inhibitions. (Figure 3.7). As a control EDTA (with a comparable K_d to Tf) was added in excess to the A β samples before and after the introduction of the various states of Tf and no significant differences were observed for the 1D ^1H -WG nor the 1D STD data taken.

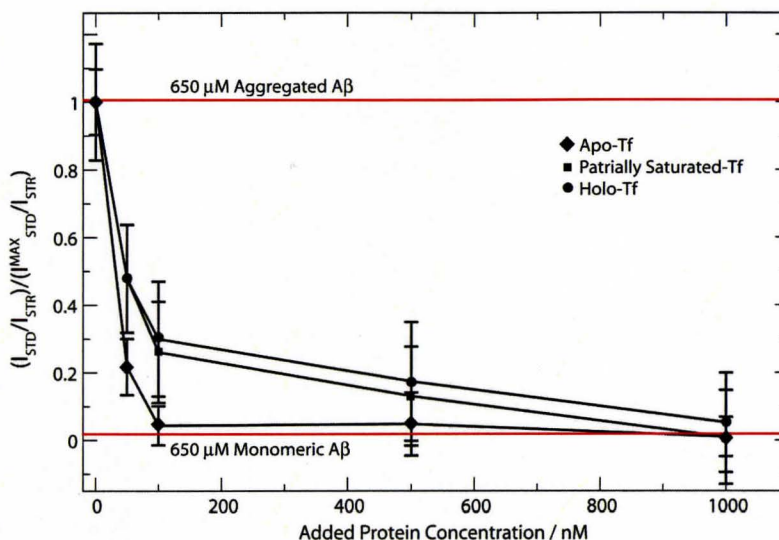


Figure 3.8 | Probing the A β Inhibitory Abilities of Tf at Various Degrees of Iron Saturation | Salt-induced aggregated A β 12-28 at 650 μM were titrated against apo-Tf (\blacklozenge), holo-Tf (\bullet) and partially saturated Tf (\blacksquare). The levels of aggregation were measured through the normalized STD intensity data $(I_{\text{STD}}/I_{\text{STR}})/(I_{\text{STD}}^{\text{MAX}}/I_{\text{STR}})$. It is observed that is only a marginal change within the inhibitory abilities between the states of Tf. This marginal error is difficult to consider due to the nature and sensitivity of the sample. The 1D STD experiments were carried out on an AV 600 MHz Bruker NMR with an inverse triple resonance multinuclear (TBI-Z) probe at 293 K.

In order to probe the inhibitory capacity of each state of Tf, a lower concentration of A β 12-28 at 650 μM was investigated in the same manner. Initiating with the addition of low nM amounts of protein (0 nM – 5 nM) to a salt-induced aggregated sample of A β 12-28, showed great instability through the analysis of 1D ^1H -STD NMR experiments (Figure 3.8). Therefore the titration was performed starting at 50 nM with a slight sacrifice on the sensitivity between the different states of Tf. Continuing the titration of

650 μM $\text{A}\beta$ with higher concentrations of apo and holo Tf, a marginal difference is observed as indicated in Figure 3.7. It appears that apo-Tf possesses a higher affinity of inhibition for the early aggregation of $\text{A}\beta$.

3.2.3 *The Effect of Residual Iron within the Sample*

Iron impurities are inevitable in all samples of any type and the presence of iron within the $\text{A}\beta$ sample may result in the initiation of oligomerization.⁸⁸ The existence of iron impurities may also have an influence on the state of Tf, specifically apo-Tf would exhibit a change in saturation. To ensure the confidence in the apo state of Tf as well as a controlled aggregation method, EDTA is added to the 1 mM of $\text{A}\beta_{12-28}$ used in the protein titration, before and after the addition of the proteins (Figure 3.6). The results of 1D ^1H -WG as well as the more quantitative 1D ^1H -STD experiments both show no change in aggregation upon the addition of an iron chelator.

Additional information from ICP analysis completed by Kevin Ferguson, B.Sc. Quality Assurance Manager at the Occupational and Environmental Health Laboratory in the Department of Chemistry at McMaster University for iron impurities within the sample resulting in \sim of 2 ng/ml of iron detected. Considering that the reported association and dissociation rate constants for $\text{A}\beta_{40}$ in the presence of Fe(III) are $2.08 \times 10^2 \text{ M}^{-1} \text{ s}^{-1}$ and $0.53 \times 10^{-3} \text{ s}^{-1}$ respectively,⁸⁹ the binding constant for ferric iron to $\text{A}\beta_{40}$ is calculated to be 2.54 μM . Therefore the trace amount of iron within the sample should not have a significant influence on the behaviour of $\text{A}\beta$.

3.3 Quantifying the Binding Potencies and the Mechanisms for the Tf, A β 12-28 Interactions

3.3.1 Tf Does Not Interact with Monomeric A β Peptides.

Thus far Tf has been shown to interrupt the monomer-oligomer exchange of A β 12-28 as presented in the above data. These disruptions are associated with the interactions between Tf and the early A β 12-28 oligomers at ratio of 1:65. The absence of STD signal or line broadening of the filtered sample after the addition of Tf rules out weak ($K_d \sim \mu\text{M} - \text{mM}$) interactions between Tf and monomeric A β 12-28. However the possibility of interactions occurring at lower K_d values ($\sim\text{nM} - \text{sub-}\mu\text{M}$) have been neglected. In order to analyze these interactions, a 125 μM sample of A β was prepared through the filtration procedure prepared for the addition of 65 μM of Tf in a similar as outline in Scheme I.

The incorporation of a *spin-lock filter* (SL) was used to suppress the large protein signal, allowing the 1D ^1H -SL-WG spectra (Figure 3.9) to essentially reflect only the monomeric species within the sample. The 1D spectrum of the 125 μM filtered A β 12-28 sample (Figure 3.9/A) shows sharp, well-defined peaks. Upon the addition of 65 μM Tf (Figure 3.9/B), there was no significant change to the original spectrum (Figure 3.9/A). The expected changes within the spectrum for a tight interaction of Tf and A β would show a decrease of intensity due to the large, 74.5 kDa protein interacting with the monomers, thus removing a portion of the monomeric population from the NMR detectable range. The results obtained show a consistent intensity level for each peak,

proving that there are no interactions involved with Tf and monomeric A β 12-28 in both K_d ranges (μM – mM and nM – sub- μM). Notable changes within the spectrum include the additional peaks that arise due to the addition of Tf that could not be fully suppressed; these have been identified within Figure 3.9.

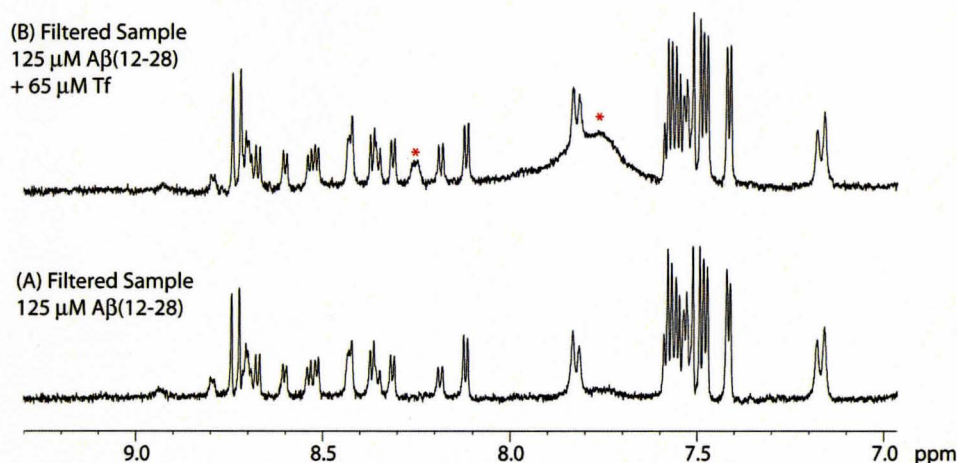
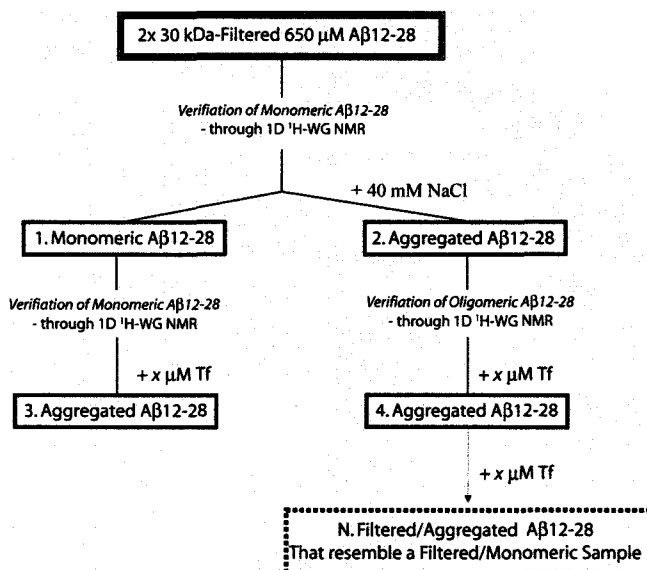


Figure 3.9 | Determination of Monomeric A β /Tf Binding Contributions | Analyzing lower K_d interactions with a ratio of 2:1 through 1D ^1H -WG-SL, taken on a 700 MHz Bruker NMR with TCI-Z cryoprobe at 293 K. (A) Filtered 125 μM A β , showing a high monomeric concentration, shown through the sharp peaks within the spectrum. (B) Filtered 125 μM of A β with the addition of 65 μM of Tf to create a 2:1 ratio. With visual analysis, there is no decrease of intensity between the two spectra and therefore concluding that there are no monomeric A β and Tf interactions that occur. The asterisks label the peaks of Tf that were not suppressed by the spin lock addition to the pulse sequence.

3.3.2 Quantitative Investigation of the Interactions between A β 12-28 and Tf through 1D ¹H-STD NMR Experiments

Through the uses of 1D ¹H-STD NMR experiments outlined in Section 3.1.1, Tf has shown to prevent the onset of salt-induced aggregation. To further examine the inhibitory mechanism a quantitative estimation of the inhibitory potencies was investigated. For this purpose 1D ¹H-STD NMR data was acquired in an alternate approach – *i.e.* Tf was titrated into salt-induced aggregates (Figure 3.10). A reference sample of the filtered A β 12-28 was once again used to verify the initial degree of aggregation. The sample procedure is outlined in Scheme IV, which is similar to initial aggregation procedure.



Scheme IV Titration of Tf against Monomeric and Oligomeric Samples of A β

Upon the addition of Tf, the STD intensity was monitored throughout the protein titration (Figure 3.10/A). The display of a typical dose-response pattern was found for the

$(I_{STD}/I_{STR})/(I_{STD}^{MAX}/I_{STR})$ values, decreasing progressively as the protein concentration increases until a plateau was reached at a Tf concentration of ~ 15 nM, resembling the degree of aggregation observed for the monomeric sample. This data can be quantified in terms of the *half-maximal inhibitory protein concentration* (IC_{50}), corresponding to the midpoint between the initial $(I_{STD}/I_{STR})/(I_{STD}^{MAX}/I_{STR})$ value and the plateau region (Figure 3.10/A). The data obtained shows that for a $650 \mu\text{M}$ sample of $A\beta_{12-28}$, the IC_{50} value was found to be ~ 4 nM.

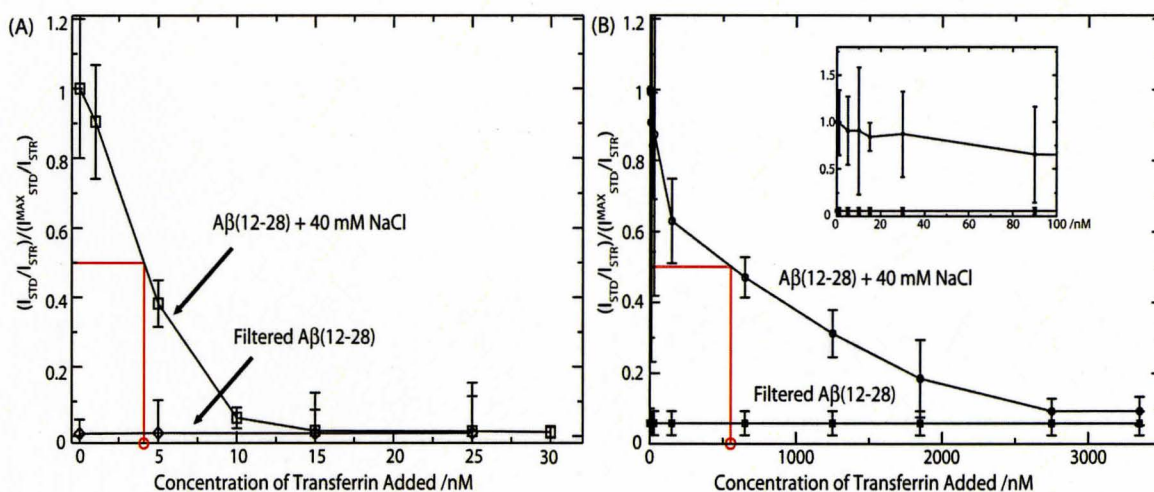


Figure 3.10 | Changes Induced with the Introduction of Tf to Aggregated $A\beta$ Samples | The influence of Tf is depicted in plot (A) comparing $650 \mu\text{M}$ of monomeric (filtered) $A\beta$, diamonds (\diamond) and an aggregated $650 \mu\text{M}$ of $A\beta$ (through the addition of 40 mM NaCl), squares (\square) are plotted with respect to the normalized STD intensity data $(I_{STD}/I_{STR})/(I_{STD}^{MAX}/I_{STR})$. The 1D STD at $650 \mu\text{M}$ of $A\beta$ experiments were carried out on a 700 MHz Bruker NMR with TCI-Z cryoprobe at 293 K. Tf targets oligomers that are formed, as indicated through the lack of change in monomeric (filtered) $A\beta$ sample. The STD intensity completely diminishes upon the addition of 15 nM Tf, resulting in an IC_{50} at 4 nM of Tf. Plot (B) Investigates this titration at a higher concentration of 1 mM of $A\beta$, thus testing the concentration dependence of Tf on $A\beta$. The experiments were carried out in the same manner with the adjustment 25 mM NaCl added to induce aggregation. It was shown that $1.85 \mu\text{M}$ of Tf diminished the STD intensity of $A\beta$, reporting an IC_{50} of 550 nM Tf. The titration at 1 mM was carried out on an AV 600 MHz Bruker NMR with a TBI-Z probe at 293 K.

To further investigate the concentration dependence of Tf a titration with a 1 mM sample of A β 12-28 was performed (Figure 3.10/B). The resulting data in comparison to the original sample conditions provided evidence of a concentration dependence associated with the IC₅₀ of Tf for A β inhibition. The IC₅₀ value of 1 mM A β was found to be 550 nM, giving a 100-fold increase from the original 650 μ M sample which had an IC₅₀ of 4 nM. Therefore, the collected data suggests that higher concentration of monomeric A β correlates with an increased fraction of oligomers within the sample, and requires higher amount of Tf for inhibition.

3.3.3 Tf Shields All Residues of Monomeric A β 12-28 from Their Interactions with A β 12-28 Oligomers

The analysis thus far utilizing STD and 1D spectral data provides information on the interaction of Tf and A β 12-28, but is limited on the shielding selectivity information involved. Monitoring the influence of 10 μ M of Tf upon an aggregated A β 12-28 sample of 650 μ M through nonselective 2D-off-resonance relaxation experiments with a 35.5° tilt angle provides a residue-specific analysis on the peptide sample. The nonselective off-resonance relaxation was measured for filtered samples, salt-induced aggregate samples and aggregated samples in the presence of Tf (Figure 3.11/A). A significant decrease of H $_{\alpha}$ -R_{35.5°,ns} relaxation rates measured for the aggregated sample of 650 μ M of A β 12-28 is observed upon the addition of 10 μ M Tf for the majority of residues, resembling the relaxation rates of the original filtered sample.

The nonselective 2D-off-resonance relaxation profiles of the added 10 μM of Tf and the filtered monomeric A β sample at 650 μM displays an excellent correlation (correlation coefficient of 0.945), supporting that the physical removal of A β oligomers from the original aggregated A β sample due to filtration is similar to the effect of the addition of Tf. This suggests that Tf has a global affect on A β 12-28, providing an equal shielding effect on the entire polypeptide.

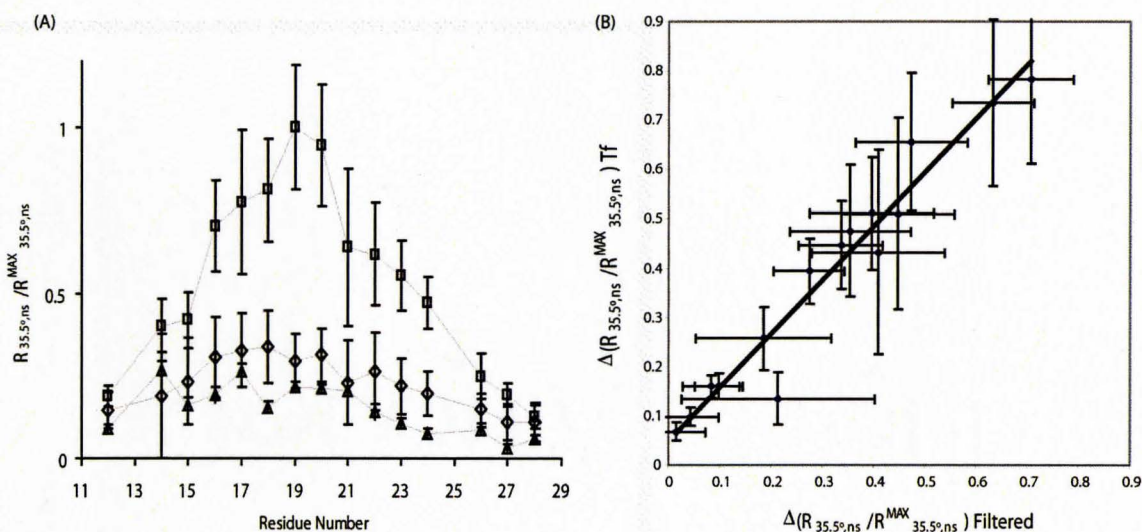


Figure 3.11 | The Global Shielding on A β 12-28 Intermediates by Tf | The plot (A) represents the response of individual residues within three sample environments; triangles (\blacktriangle) filtered 650 μM of monomeric A β 12-28, squares (\square) 650 μM of A β 12-28 with the introduction of 40 mM NaCl to induce aggregation and the diamonds (\diamond) 650 μM of aggregated A β with added 10 μM of Tf. The plotted rates in (B) were all normalized to show a direct correlation between the monomeric 650 μM of A β on the x-axis against an aggregated sample with the addition of 10 μM Tf on the y-axis. The 2D ORR experiment was run on a 700 MHz Bruker NMR with TCI cryoprobe at 293 K

3.4 The Mechanism for the Inhibition by Tf of the A β 12-28 Oligomerization

3.4.1 Tf Inhibits the Early A β Oligomerization through a Competitive Mechanism

There are two plausible mechanisms that could potentially account for the inhibitory action of Tf on A β aggregation. Both mechanisms have been observed before for other systems. The molecular chaperone Hsp104 targets the oligomeric population of the Sup35 prion-peptide and destabilizes it until the monomeric population has been recovered,⁷³ whereas *apolipoprotein E* (ApoE) allele 3, targets an oligomeric intermediate through binding to oligomeric species preventing further aggregation.⁹⁰ These possible mechanisms have been classified as *destabilization* (Hsp104 case) and *competitive* (ApoE3 case) mechanism. If Tf acts through a *destabilizing mechanism*, it would be expected that Tf addition to the aggregated sample, would restore the monomeric state. However, if Tf acts through a *competitive mechanism*, it would be expected that oligomers are still present after adding Tf. (Figure 3.12)



$$\text{where } i n = i' n' \text{ and } i' < i$$

Figure 3.12 | The Two Most Probable Mechanism for the Inhibition of A β Aggregation by Tf | Based on the nucleated-dependent polymerization model with focus on the earlier stages of aggregation two options are probable. A destabilization mechanism that breaks down the oligomeric species formed during aggregation or a competitive mechanism that coats the oligomeric species preventing further monomeric additions.

In addition, if Tf acts through a *destabilization mechanism* a stoichiometric amount of Tf would not be required. In a *competitive mechanism*, Tf poses a limited stoichiometric amount, binding specifically to the targeted early intermediates, therefore not restoring the aggregates to their monomeric form, but coating them against further aggregation. To investigate the differences between the two distinct mechanisms, the size-dependent detection limit of solution-state NMR is exploited. The outline of the sample history is similar to that of Scheme I, with a higher salt concentration was added to ensure a higher concentration of oligomers within the aggregated sample (Figure 3.13).

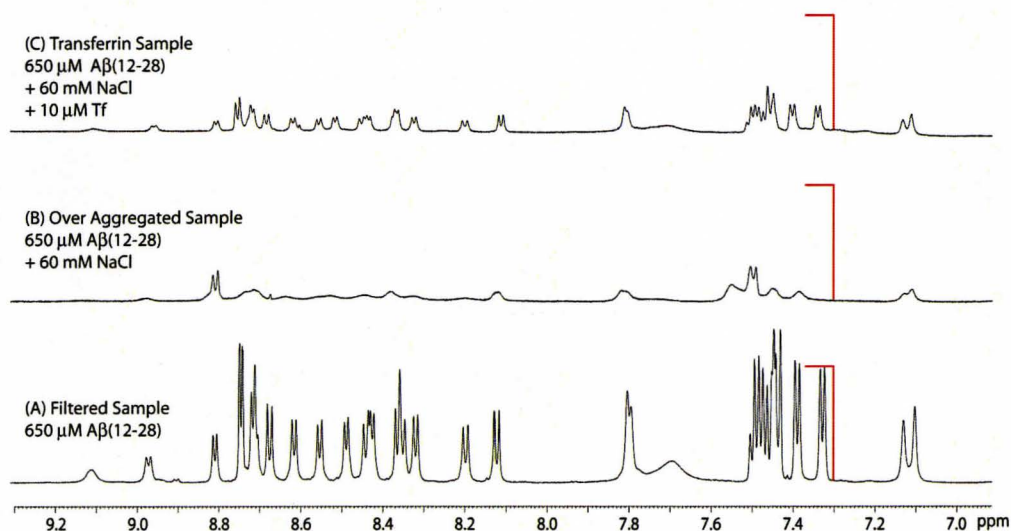


Figure 3.13 | Tf Does Not Destabilize Oligomeric A β Intermediates | Two postulating mechanisms are feasible; a competitive mechanism and a destabilization mechanism. (A) Standard filtered 650 μ M of A β 1D 1 H-WG spectrum. (B) Introduction of 60 mM NaCl, thus over-aggregating the sample, which is observed by the extreme line broadening. (C) 10 μ M of Tf is added to the over-aggregated A β sample, noting that the line broadening has improved, but the peak heights remain less intense, therefore providing evidence of a ‘competitive’ mechanism occurring in contrast to the ‘destabilizing’ mechanism. 1D 1 H-WG experiments were all taken on a 700 MHz Bruker NMR with TCI cryoprobe at 293 K.

The initial spectrum represents the monomeric form of A β 12-28. This spectrum was then compared to the spectrum recorded after adding 60 mM NaCl where the sample was purposely over-aggregated to produce a greater population of A β 12-28-oligomers (indicated by the decrease of peak intensity and an increase of peak broadening). After the addition of Tf to the aggregated sample (Figure 3.11/C) most peaks were influenced however, the monomeric signal was not restored to its original state (Figure 3.13/B). Tf (MW 78 kDa) is outside the NMR detectable limit, therefore only the monomeric A β 12-28 can be detected. The results suggest a *competitive mechanism*, in which Tf binds oligomers, prevents monomeric addition and the formation of aggregates.

3.5 The Structural Analysis on the Intermediates Targeted by Tf for the Inhibition of A β 12-28

3.5.1 Secondary Structural Analysis through 2D NOESY NMR Experiments

Knowing that Tf inhibits A β 12-28 oligomerization through a competitive mechanism in which it targets oligomeric intermediates, the next step was to characterize the oligomeric intermediates. This was done using 2D NOESY NMR experiments detect the dipolar (through space) interactions that provide structural information by correlating the distances to the NOEs observed within the spectrum.⁹¹ NOESY spectra were acquired for the reference samples representing a monomeric A β sample and an aggregated A β sample with and without Tf (Figure 3.14). The filtered-monomeric A β 12-28 sample and

Tf added sample NOESY spectra were directly compared against the NOESY data for the salt-induced aggregated sample of A β 12-28.

The comparison of the spectra shows that upon filtration several NOEs observed in the aggregated sample disappear from the spectrum. The change of NOEs may result from non-specific effects namely the viscosity change upon removal of the larger oligomer retained by this effect. This property can be ruled out, for it has been shown that the diffusion coefficient of A β 12-28 does not significantly change upon filtration.⁴⁰ Therefore, the NOEs that are removed through the act of filtration arise from transfer cross-relaxation⁷² predominantly from the soluble oligomers, which have the potential to provide useful structural information about the A β 12-28 aggregates. However, to differentiate between intermolecular and intramolecular interactions a full structural determination is required, involving isotope-editing and filtering methods for the aggregated sample. This means that the data collected so far can be analyzed for qualitative data of the filtration-dependent NOEs. The NOEs present in the aggregated samples of A β 12-28 but absent in the filtered non-aggregated samples correspond to residues D₂₃V₂₄G₂₅S₂₆ that form a cluster of medium-ranged NOEs (V₂₄ H _{α} to S₂₆ H_N, E₂₂ H _{α} to S₂₆ H_N, E₂₂ H _{α} to V₂₄ H_N and D₂₃ H _{α} G₂₅ H_N). These H _{α} - H_N sequential contacts characterize the formation of helical (α and/or 3₁₀) conformations.⁹¹

Upon filtration on the aggregated A β 12-28 sample, the clusters of helical residues representing pre-nuclear oligomers are removed. The addition of Tf to the aggregated sample of A β 12-28 was also monitored through 2D NOESY NMR to reveal a similar effect to filtration resulting in the cluster of helical NOEs being removed from the

spectrum. This in turn provides solid evidence for the inhibition of the early intermediates of A β 12-28 oligomerization by Tf. This data also provides new evidence on the targeted oligomers during this inhibition, which adopt a helical confirmation upon salt-induced aggregation. However, based on the NOE data alone, we cannot rule out the presence of alternative non-helical structure for the oligomers.

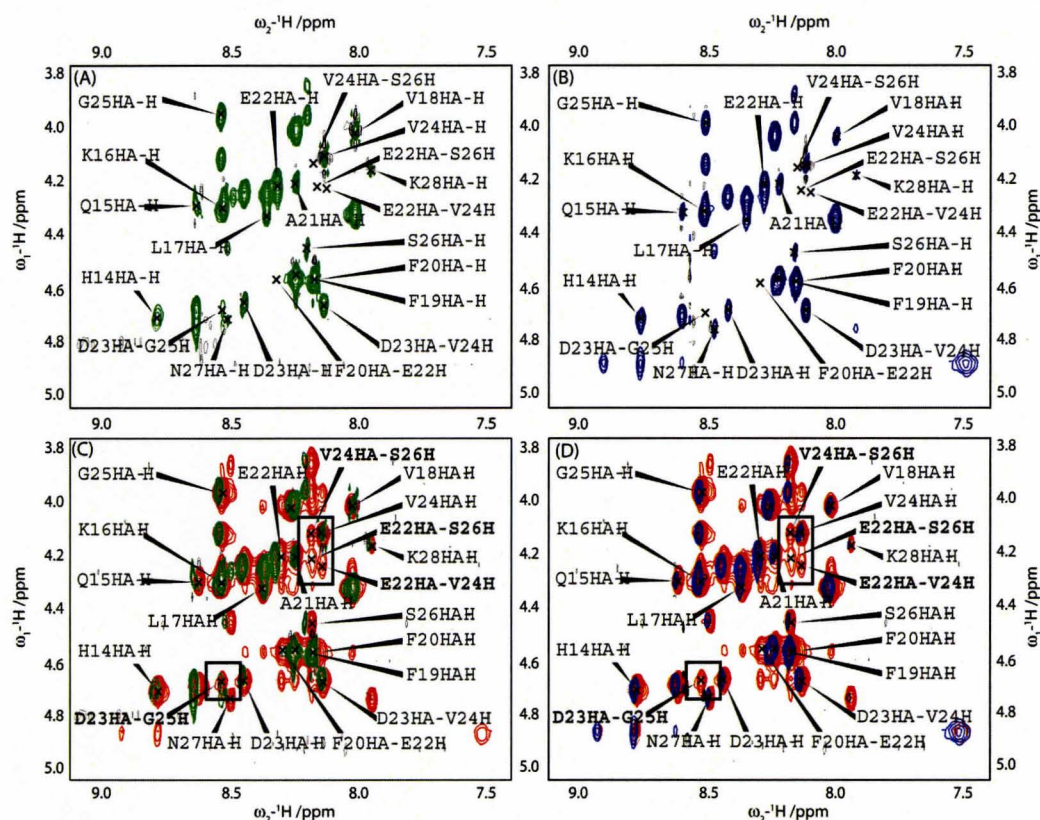


Figure 3.14 | Structural Analysis of Targeted Intermediate in A β Inhibition | 2D NOESY NMR experiments were performed for qualitative structural analysis on 650 μ M of A β 12-28 in 50 mM of deuterated sodium acetate buffer with 10% D₂O and filtered at a 30 kDa. Spectrum A (blue) described the behavior of the filtered A β 12-28 sample, with minimal contours. Spectrum B (green) shows the NOEs that are produced for the added Tf sample of aggregated A β 12-28. Spectrum C and D is the overlay comparison of A and B to the aggregated sample of A β 12-28 (red). New contours are identified in the aggregated sample that does not appear in the filtered or the Tf added samples. The NOE data was collected on a 700 MHz Bruker NMR with TCI cryoprobe at 293 K

3.5.2 Analysis of A β Oligomeric Binding to Tf through CD Spectroscopy

Upon the onset of aggregation of the amyloid peptide several conformational changes occur as hypothesized with the structural transition from α -helical to β -sheet.⁴¹ A reliable probe for structural determination is CD spectroscopy. The structural changes of a filtered-monomeric A β 12-18 sample at 650 μ M in the presence and absence of 10 μ M of Tf were monitored for a salt gradient ranging from 0 mM to 40 mM NaCl (Figure 3.15). The samples prepared through Scheme II for STD detection in Figure 3.5 in were used for CD analysis. The spectra are plotted as molar ellipticity (degree \cdot cm²/dmol) of the sample against a range of wavelengths between 190 nm – 270 nm at 298 K.

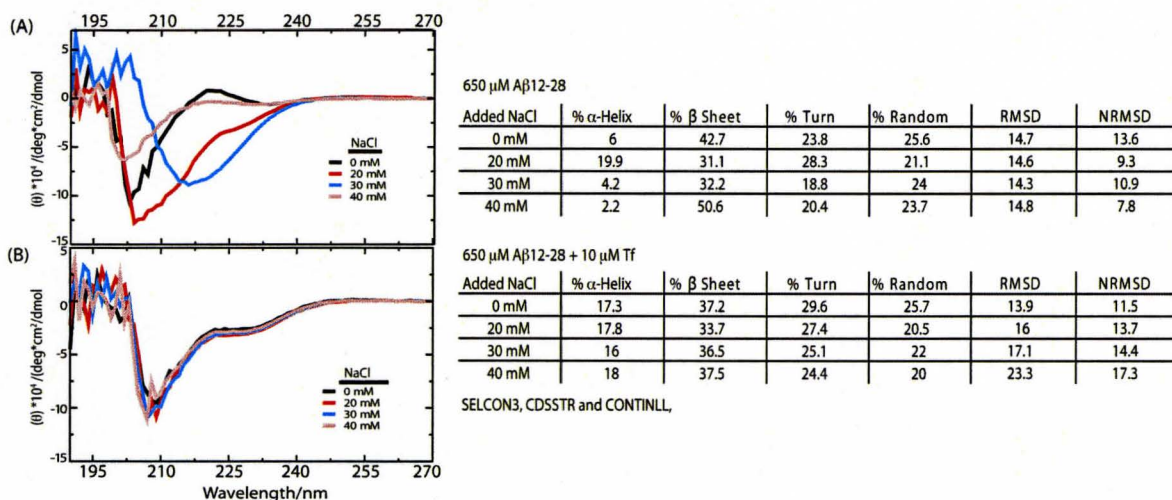


Figure 3.15 | CD Spectroscopy for Structural Analysis upon Aggregation and Inhibition of A β | A salt titration previously performed by NMR and is now analyzed through CD. The A β 12-28 sample at 650 μ M with and without Tf was aggregated with various concentrations of salt. At each stage of the titration a 30-day stabilization period was given. (A) 650 μ M of A β 12-28 without Tf, exhibits great conformational changes throughout the salt additions. (B) Addition of Tf to the monomeric A β 12-28 shows a resistance to structural changes. The data was obtained on a far-UV AVIV circular dichroism model 410 at a range of 180 - 270 nm at 298 K

The CD spectrum of A β 12-28 in the absence of Tf exhibits great conformational change. The percentages of secondary structures were calculated resulting in an increase of helical intermediates with the addition of 20 mM NaCl and an increase of β -sheet structure with the addition of 40 mM NaCl, which is what is expected from previous studies.^{42,72} These samples were taken after 60 days from initial preparation. These samples were proven to be stable with respect to the addition of salt for aggregation. However these samples underwent a higher degree of physical manipulation during the transfer between the NMR tubes to the CD cell. This physical involvement may seem minor, but may have an influence on the structural identification.

The same salt titration was used against the monomeric A β 12-28 sample in the presence of Tf. The added Tf was able to withstand the structural changes that occur during A β aggregation. The calculated secondary structures reinforce the argument that Tf prevents any structural changes within A β . However, the measurement of CD involves a global reading, averaging the secondary structures within the sample. As a blank subtraction the CD spectrum of Tf alone was taken. This potentially removes the contributions of Tf however the interactions of A β with Tf may cause conformational changes that are not accounted, therefore no structural analysis can be made.

Conclusions

Chapter 4

Conclusions

4.0 Tf Inhibits Early Oligomerization in the A β Self-Association Process and Key Determinates of Inhibition are Contained within the 12-28 Region of the A β Peptide

Through the qualitative line-width analysis of 1D ^1H -WG NMR spectra, (Figure 3.4), Tf was shown to decrease the transverse relaxation rates of aggregated A β 12-28, sharpening the peak width as observed for a filtered, largely monomeric A β sample (Figure 3.4/A). This is an indication of the disruption of dynamic exchange between the monomeric A β and oligomeric intermediates formed during the early stages of aggregation. A similar disruption of monomer – oligomer dynamic exchange was also observed when Tf was added prior to the formation of A β aggregates through the titration of salt to mimic varying degrees of aggregation. The salt titration was monitored through 1D ^1H -STD NMR spectra, conferring that Tf inhibits the onset of aggregation for the A β 12-28 sample. (Figure 3.5).

4.1 The Inhibitory Effect of Tf on Early A β Aggregation is Not Iron Mediated

For the purpose of investigating iron sequestration as a possible inhibitory process of the early stages of A β self-association by Tf, EDTA is utilized as a control against Tf. Aggregation detection by 1D ^1H -STD showed that EDTA had no influence on the degree of A β aggregation under our sample conditions. As an additional control Tf was also

added to each sample, (Figure 3.6), thus providing further evidence that Tf influences the aggregation level of A β in an iron-independent mechanism.

The residual iron was also tested through ICP analysis, which determined a 35.8 nM concentration of iron (including both of ferric and ferrous iron) within the sample. This value is below the dissociation value reported for iron to initiate A β 40 aggregation (2.54 μ M), under our experimental conditions.

4.2 The Degree of Iron Saturation in Tf Does Not Significantly Affect the Tf Inhibitory Potency

Through 1D 1 H-STD it was shown that each state of Tf –*i.e.* holo-Tf and apo-Tf is able to inhibit the early aggregation of A β 12-28 (Figure 3.7). The potency of each state was quantified through IC₅₀ values that are within error from each other (Figure 3.7). Repeating the titrations at lower A β concentrations corresponded lower IC₅₀ values, (Figures 3.8 and 3.10), with only marginal changes observed for the various Tf states.

The residual iron within the sample found at 35.8 nM is above the K_d value reported for Tf - ferric iron binding (K_d ~ 10⁻²⁰ M). This potential binding was tested with the additional control of EDTA (K_d ~ 10⁻²³ M), introduced in excess before and after the treatment of apo-Tf to the aggregated A β sample, no significant changes were observed. Data not specifically shown, EDTA was implemented as part of the detection of protein titration in Figure 3.7.

4.2.1 *The Potency of the Inhibition of A β Oligomerization is Below the Reported Tf Concentration in CSF*

The potency of the inhibitory abilities of Tf were tested through 1D ^1H -STD experiments (Figure 3.10) that resulted in an IC_{50} of approximately 4 nM of Tf for a 650 μM sample of A β 12-28. This value is well below the reported physiological levels within the plasma 38 μM ,⁶⁹ as well as within the CSF, 170 nM.⁶⁹ To evaluate the range of error in the IC_{50} values, duplicated experiments are compared (Figure 3.8), leading to an IC_{50} range of 4 nM - 40 nM, still remains below the reported concentration in the CSF. The concentration of A β reported in the CSF for AD patients of ages ranging from 45-85 years old, is 825 pM for A β 40 and 80 pM for A β 42,¹⁹ entailing an excess of Tf available for A β inhibition for physiological conditions.

4.3 *Tf Utilizes a Competitive Mechanism for the Inhibition of the Early Stages of A β Oligomerization*

Two viable mechanisms for the inhibition of early A β aggregation were considered for Tf (Figure 3.12). The data collected in 1D ^1H -WG and 1D-STD is consistent with the model in which Tf acts through a *competitive mechanism*, targeting oligomeric A β intermediates, to avoid further additions of monomeric A β to form larger oligomers and eventually the *critical nucleus*.

4.3.1 The Mechanism of Inhibition Does Not Imply the Destabilization of A β Oligomeric Intermediates

The destabilization of oligomeric intermediates entails an inhibitor without a concentration dependence, by means of recycling to continually destabilize the newly formed oligomeric A β intermediates. In addition, 1D ^1H -WG NMR data obtained for a highly concentrated oligomeric A β 12-28 sample has shown that Tf added was unable to restore the monomeric concentration (Figure 3.13) therefore suggesting the inability to continually destabilize the oligomeric contributions.

4.3.2 Tf Does Not Interact with the Monomeric Portion of A β

No interactions were observed between Tf – monomeric A β at comparable ratio through 1D ^1H -WG NMR (Figure 3.9). This experiment targeted the possibility of tightly bound interactions that would not have been detectable in previous experiments. The lack of change of the filtered A β monomeric peak shape and intensity upon the addition of Tf provided evidence of the absence of tight interactions occurring between Tf and monomeric A β .

4.3.3 Oligomeric Concentration Dependence is Exhibited for Tf Inhibition

The Tf inhibitory mechanism targets pre-nuclear A β oligomeric species. This is observed through the concentration dependence that was revealed by the comparison of protein titrations against aggregated A β samples at various peptide concentrations (Figure

3.10). Higher concentrations of A β entail a higher population of oligomers formed during aggregations, correlating to an increase of Tf concentration required for inhibition. The increase of Tf IC₅₀ values observed at higher concentrations of A β also reinforces the observation of a *competitive* inhibitory mechanism in which Tf binds to A β oligomers.

4.4 All Amino Acid Residues within the Oligomeric Species are Entirely Shielded by the Inhibitory Mechanism of Tf

2D-ORR NMR provided residue-resolution analyses which have shown that all A β ₁₂₋₂₈ amino acid residues are equally shielded upon the interaction with Tf (Figure 3.11). This indicates that Tf prevents all residues within the A β -oligomeric intermediates from further aggregation. This conclusion was supported by the direct correlation of ORR data for the physical removal of oligomeric A β through filtration and for the addition of Tf.

Future Work

Chapter 5

Future Work

5.0 Investigation of Iron - A β 12-28 Binding

Interactions between ferric iron and A β 40 have been identified as binding to residues His6, Tyr10, His13 and His14.^{57,92} However these results have not been translated to the fragmented A β 12-28. Detection of metalloprotein by NMR focuses on the metal ion as a point of discontinuity in the network of coherence transfers. Metal-ligand coupling can be detected by heteronuclear NMR –*i.e.* metal-proton correlation producing cross peaks of metal-nucleus-protein coupling (MXCH). Restrictions exist with metal nuclei with a $I > \frac{1}{2}$ producing a quadrupolar relaxation that may broaden peaks beyond detection. The investigation of ferric iron in particular includes paramagnetic properties that entails a large magnetic moment and a relaxation time ranging from $10^{-13} - 10^{-18}$ s.⁹³

These two properties can be capitalized for the identification of the binding sites of iron to the peptide. The bound metal is known to produce a ‘binding zone’ around the targeted amino acid. This binding zone produced affects the line-width of the peaks with the reciprocal of the 6th power to the distance to the metal-nucleus.⁹⁴ Therefore initially as seen as qualitative, 1D ¹H-WG NMR experiments can be utilized. Another property to be considered is the onset of *hyperfine* shifts. This is an additional contributions to the chemical shift experienced upon the presence of unpaired electrons, which is an

indication of metal binding, but will also create difficulties with the elucidations of the A β 12-28 peptide spectrum.

The use of heteronuclear NMR will aid in the elucidation of the newly implemented chemical shifts, but will also decrease relaxation rates. The dipolar coupling is dependent upon the square of the gyromagnetic ratio. The switch of detection from ^1H to ^{13}C creates a decrease of the relaxation rates by a factor of six.⁹³ There is a draw back with the loss of sensitivity. However with availability of a wide range of multi-dimensional NMR techniques much information on the structure can be obtained.

5.1 Verification of Apo-Tf and Holo-Tf Species

A controlled pH environment is essential for the monitoring A β aggregation. However upon the introduction of Tf, the issue of conformational changes upon the fluctuation of pH for the structure of Tf may influence the inhibition of A β aggregation. As a quick and efficient verification UV absorbance can be measured. It is known that the structure of Tf produces a strong absorption at ~ 280 nm and once tyrosine loosens the phenolic proton, which is assumed to be apart of the transition from holo to apo state, the UV absorbance at 295 nm and 245 nm are dramatically increased.⁹⁵ Typically the concentration of protein required is in the mM range which may be difficult to utilize throughout protein titrations. However, stock solutions prepared for these proteins can be verified with this simple detection method.

5.2 Relevance of Inhibition upon the involvement of A β 42

Thus far all experimental detections have been focused on the actions of the fragmented A β 12-28, which is known to hold key determinates of the full-length peptide. For a complete confirmation on the validity of the fragmented peptide the interactions between Tf and the full-length A β 42 can be monitored. However, differences between the length and the dynamics of the peptides have to be taken into consideration for the choice of detection techniques. Observations made through the STD NMR analysis during an A β salt-gradient (Figure 3.6) resulted in a more quantitative measure of aggregation. Due to the transient nature of the oligomers formed by the longer A β 42, STD experiments are unable to quantify the longer peptide. However, A β 42 self-association can be monitored through the signal loss occurring over time after sample preparation in a 1D Watergate experiment incorporating long spin lock pulse with sufficient strength prior to acquisition to suppress the residual protein signal. Detection through 1D time-profiles for A β 42 can be acquired in the presence and absence of Tf. The rate of aggregation would occur without induction due to the rapid aggregation rate, however to obtain an original monomeric sample may pose to be difficult.

5.3 Utilization of Various Detection Techniques to Expand the Limit of Detection

The complexity in working with the full-length A β 40/A β 42 peptides is due to the sheer size the oligomeric intermediates formed. Protein NMR has been developing at an exponential rate, however dealing with a large entity; Tf ~ 78 kDa creates difficulties

with the NMR detection. To aid with this detection problem additional detection techniques are involved. Thus far the implementation of CD spectroscopy has allowed an overall analysis of the secondary structures versus the focused detection of NMR.

Upon further aggregation to the level of fibril formation, the lack of mobility within the sample poses a problem with both solution-state NMR as well as CD spectroscopy. Therefore the next progression for detection could be electron microscopy (EM). This detection results in an image taken on the scale of angstroms. An image of fibrillar formation within the samples will be a clear observation; also effects of the Tf to the aggregated sample can be tested.

5.4 Determination of the Specific Binding Sites

Determination of the specific binding sites on Tf and A β would be highly beneficial for a potential drug binding site and furthering the understanding the aggregation process of A β . Testing a variety of segments of the peptide is the technique that was initiated within this research, however changes within the binding protein could also be considered. Initially the domains of Tf can be analyzed individually. There have been many studies that isolate the individual domains of Tf to test binding abilities.

There is a hydrophobic, helical region at the bottom cleft of each domain that is thought to play an integral role in the bind to the TfR. To target this region the mutagenesis can be preformed on the peptide to test for specific binding. The aspect of NMR elucidation may come into play for the identification of the binding site as well.

This job may pose to be difficult, but with isotopic-labeling and multi-dimensional NMR, data can be obtained on the structure of Tf.

5.5 Comparison to Other Common Plasma Proteins

Tf is one of many plasma proteins that result in the inhibition of A β aggregation. The most studied protein is human serum albumin. It is present in both the plasma as well as the CSF in significantly higher concentrations than Tf.⁶⁹ A direct comparison for inhibition mechanisms would gain insight on perhaps a general mechanism that could be implemented as a treatment for aggregation. However comparisons involving the highly sensitive peptide samples can be difficult. Most previously published work is hard to directly compare with the change of buffer, temperature and even batch. Therefore to achieve an accurate comparison for the plasma proteins the sample treatment procedures have to stem from the same original batch. Experiments following similar procedures as outlines in this study have been performed for albumin and at various length of A β .^{83,96} Thus far the results that have been reported are similar to what was found for Tf, though a comparison involving an experimental setup that involved both proteins would reveal a true comparison.

Reference

- 1 Alzheimer, A. (1907) Ueber eine eigenartige Erkrankung der Hirnrinde. *Centralblatt für Nervenheilkunde und Psychiatrie* 30, 177-179
- 2 Chiang, P.K. et al. (2008) The many faces of amyloid beta in Alzheimer's disease. *Curr Mol Med* 8 (6), 580-584
- 3 Sano, M. et al. (2008) Preventing Alzheimer's disease : separating fact from fiction. *CNS Drugs* 22 (11), 887-902
- 4 Verdile, G. et al. (2004) The role of beta amyloid in Alzheimer's disease: still a cause of everything or the only one who got caught? *Pharmacol Res* 50 (4), 397-409
- 5 Glenner, G.G. et al. (1984) The amyloid deposits in Alzheimer's disease: their nature and pathogenesis. *Appl Pathol* 2 (6), 357-369
- 6 Atwood, C.S. et al. (2003) Amyloid-beta: a chameleon walking in two worlds: a review of the trophic and toxic properties of amyloid-beta. *Brain Res Brain Res Rev* 43 (1), 1-16
- 7 van der Zee, J. et al. (2008) Invited article: the Alzheimer disease-frontotemporal lobar degeneration spectrum. *Neurology* 71 (15), 1191-1197
- 8 Polverino de Laureto, P. et al. (2003) Protein aggregation and amyloid fibril formation by an SH3 domain probed by limited proteolysis. *J Mol Biol* 334 (1), 129-141
- 9 Baumketner, A. et al. (2008) Role of the familial Dutch mutation E22Q in the folding and aggregation of the 15-28 fragment of the Alzheimer amyloid-beta protein. *Proc Natl Acad Sci U S A* 105 (16), 6027-6032
- 10 Markesbery, W.R. (1997) Oxidative stress hypothesis in Alzheimer's disease. *Free Radic Biol Med* 23 (1), 134-147
- 11 Haass, C. and Selkoe, D.J. (2007) Soluble protein oligomers in neurodegeneration: lessons from the Alzheimer's amyloid beta-peptide. *Nat Rev Mol Cell Biol* 8 (2), 101-112
- 12 Yu, W.H. et al. (2005) Macroautophagy--a novel Beta-amyloid peptide-generating pathway activated in Alzheimer's disease. *J Cell Biol* 171 (1), 87-98
- 13 Sastre, M. et al. (2001) Presenilin-dependent gamma-secretase processing of beta-amyloid precursor protein at a site corresponding to the S3 cleavage of Notch. *EMBO Rep* 2 (9), 835-841
- 14 Shoji, M. et al. (1992) Production of the Alzheimer amyloid beta protein by normal proteolytic processing. *Science* 258 (5079), 126-129
- 15 Haass, C. et al. (1992) Amyloid beta-peptide is produced by cultured cells during normal metabolism. *Nature* 359 (6393), 322-325
- 16 Seubert, P. et al. (1992) Isolation and quantification of soluble Alzheimer's beta-peptide from biological fluids. *Nature* 359 (6393), 325-327
- 17 Bates, K.A. et al. (2008) Clearance mechanisms of Alzheimer's amyloid-beta peptide: implications for therapeutic design and diagnostic tests. *Mol Psychiatry*

- 18 Bornebroek, M. et al. (2003) Hereditary cerebral hemorrhage with amyloidosis Dutch type (A β PP 693): decreased plasma amyloid- β 42 concentration. *Neurobiol Dis* 14 (3), 619-623
- 19 Tapiola, T. et al. (2000) Three-year follow-up of cerebrospinal fluid tau, beta-amyloid 42 and 40 concentrations in Alzheimer's disease. *Neurosci Lett* 280 (2), 119-122
- 20 Nagele, R.G. et al. (2004) Contribution of glial cells to the development of amyloid plaques in Alzheimer's disease. *Neurobiol Aging* 25 (5), 663-674
- 21 Kuo, Y.M. et al. (1996) Water-soluble A β (N-40, N-42) oligomers in normal and Alzheimer disease brains. *J Biol Chem* 271 (8), 4077-4081
- 22 Burdick, D. et al. (1992) Assembly and aggregation properties of synthetic Alzheimer's A β /beta amyloid peptide analogs. *J Biol Chem* 267 (1), 546-554
- 23 Mastrangelo, I.A. et al. (2006) High-resolution atomic force microscopy of soluble A β 42 oligomers. *J Mol Biol* 358 (1), 106-119
- 24 Gong, Y. et al. (2003) Alzheimer's disease-affected brain: presence of oligomeric A β ligands (ADDLs) suggests a molecular basis for reversible memory loss. *Proc Natl Acad Sci U S A* 100 (18), 10417-10422
- 25 Hepler, R.W. et al. (2006) Solution state characterization of amyloid beta-derived diffusible ligands. *Biochemistry* 45 (51), 15157-15167
- 26 Wirths, O. et al. (2004) A modified beta-amyloid hypothesis: intraneuronal accumulation of the beta-amyloid peptide--the first step of a fatal cascade. *J Neurochem* 91 (3), 513-520
- 27 Fawzi, N.L. et al. (2007) Determining the critical nucleus and mechanism of fibril elongation of the Alzheimer's A β (1-40) peptide. *J Mol Biol* 365 (2), 535-550
- 28 Lesne, S. et al. (2006) A specific amyloid- β protein assembly in the brain impairs memory. *Nature* 440 (7082), 352-357
- 29 Walsh, D.M. et al. (1999) Amyloid beta-protein fibrillogenesis. Structure and biological activity of protofibrillar intermediates. *J Biol Chem* 274 (36), 25945-25952
- 30 Lord, A. et al. (2006) The Arctic Alzheimer mutation facilitates early intraneuronal A β aggregation and senile plaque formation in transgenic mice. *Neurobiol Aging* 27 (1), 67-77
- 31 Morimoto, A. et al. (2004) Analysis of the secondary structure of beta-amyloid (A β 42) fibrils by systematic proline replacement. *J Biol Chem* 279 (50), 52781-52788
- 32 Lazo, N.D. et al. (2005) On the nucleation of amyloid beta-protein monomer folding. *Protein Sci* 14 (6), 1581-1596
- 33 Kim, W. and Hecht, M.H. (2006) Generic hydrophobic residues are sufficient to promote aggregation of the Alzheimer's A β 42 peptide. *Proc Natl Acad Sci U S A* 103 (43), 15824-15829
- 34 Baumketner, A. and Shea, J.E. (2007) The structure of the Alzheimer amyloid beta 10-35 peptide probed through replica-exchange molecular dynamics simulations in explicit solvent. *J Mol Biol* 366 (1), 275-285

- 35 Baumketner, A. and Shea, J.E. (2006) Folding landscapes of the Alzheimer amyloid-beta(12-28) peptide. *J Mol Biol* 362 (3), 567-579
- 36 Dobson, C.M. (2003) Protein folding and misfolding. *Nature* 426 (6968), 884-890
- 37 Antzutkin, O.N. et al. (2003) Site-specific identification of non-beta-strand conformations in Alzheimer's beta-amyloid fibrils by solid-state NMR. *Biophys J* 84 (5), 3326-3335
- 38 Dobson, C.M. (1999) Protein misfolding, evolution and disease. *Trends Biochem Sci* 24 (9), 329-332
- 39 Arimon, M. et al. (2005) Fine structure study of Abeta1-42 fibrillogenesis with atomic force microscopy. *Faseb J* 19 (10), 1344-1346
- 40 Jarvet, J. et al. (2003) A left-handed 3(1) helical conformation in the Alzheimer Abeta(12-28) peptide. *FEBS Lett* 555 (2), 371-374
- 41 Baumketner, A. et al. (2006) Amyloid beta-protein monomer structure: a computational and experimental study. *Protein Sci* 15 (3), 420-428
- 42 Danielsson, J. et al. (2005) The Alzheimer beta-peptide shows temperature-dependent transitions between left-handed 3-helix, beta-strand and random coil secondary structures. *Febs J* 272 (15), 3938-3949
- 43 Hardy, J. (1999) The shorter amyloid cascade hypothesis. *Neurobiol Aging* 20 (1), 85; discussion 87
- 44 Urbanc, B. et al. (2004) In silico study of amyloid beta-protein folding and oligomerization. *Proc Natl Acad Sci U S A* 101 (50), 17345-17350
- 45 Pratico, D. (2008) Oxidative stress hypothesis in Alzheimer's disease: a reappraisal. *Trends Pharmacol Sci*
- 46 de Groot, N.S. et al. (2006) Mutagenesis of the central hydrophobic cluster in Abeta42 Alzheimer's peptide. Side-chain properties correlate with aggregation propensities. *Febs J* 273 (3), 658-668
- 47 Fraser, P.E. et al. (1991) pH-dependent structural transitions of Alzheimer amyloid peptides. *Biophys J* 60 (5), 1190-1201
- 48 Ferrone, F. (1999) Analysis of protein aggregation kinetics. *Methods Enzymol* 309, 256-274
- 49 Oosawa, F. (1975) The effect of field fluctuation on a macromolecular system. *J Theor Biol* 52 (1), 175-186
- 50 Powers, E.T. and Powers, D.L. (2008) Mechanisms of protein fibril formation: nucleated polymerization with competing off-pathway aggregation. *Biophys J* 94 (2), 379-391
- 51 Xue, W.F. et al. (2008) Systematic analysis of nucleation-dependent polymerization reveals new insights into the mechanism of amyloid self-assembly. *Proc Natl Acad Sci U S A* 105 (26), 8926-8931
- 52 Roher, A.E. et al. (2000) Oligomerization and fibril assembly of the amyloid-beta protein. *Biochim Biophys Acta* 1502 (1), 31-43
- 53 Kirkitadze, M.D. et al. (2001) Identification and characterization of key kinetic intermediates in amyloid beta-protein fibrillogenesis. *J Mol Biol* 312 (5), 1103-1119

- 54 Crouch, P.J. et al. (2005) Copper-dependent inhibition of human cytochrome c oxidase by a dimeric conformer of amyloid-beta1-42. *J Neurosci* 25 (3), 672-679
- 55 Samudralwar, D.L. et al. (1995) Elemental imbalances in the olfactory pathway in Alzheimer's disease. *J Neurol Sci* 130 (2), 139-145
- 56 Molina-Holgado, F. et al. (2007) Metals ions and neurodegeneration. *Biometals* 20 (3-4), 639-654
- 57 Atwood, C.S. et al. (2000) Characterization of copper interactions with alzheimer amyloid beta peptides: identification of an attomolar-affinity copper binding site on amyloid beta1-42. *J Neurochem* 75 (3), 1219-1233
- 58 (2008) RCSB Protein Data Bank. (Vol. 2008), Rutgers, the State University of New Jersey and San Diego Supercomputer Center (SDSC)
- 59 Beard, J.L. et al. (1993) Iron in the brain. *Nutr Rev* 51 (6), 157-170
- 60 Moos, T. (1996) Immunohistochemical localization of intraneuronal transferrin receptor immunoreactivity in the adult mouse central nervous system. *J Comp Neurol* 375 (4), 675-692
- 61 Lieu, P.T. et al. (2001) The roles of iron in health and disease. *Mol Aspects Med* 22 (1-2), 1-87
- 62 Aisen, P. and Listowsky, I. (1980) Iron transport and storage proteins. *Annu Rev Biochem* 49, 357-393
- 63 Wally, J. et al. (2006) The crystal structure of iron-free human serum transferrin provides insight into inter-lobe communication and receptor binding. *J Biol Chem* 281 (34), 24934-24944
- 64 Grossmann, J.G. et al. (1993) Metal-induced conformational changes in transferrins. *J Mol Biol* 229 (3), 585-590
- 65 He, Q.Y. et al. (1999) Dual role of Lys206-Lys296 interaction in human transferrin N-lobe: iron-release trigger and anion-binding site. *Biochemistry* 38 (30), 9704-9711
- 66 Peterson, N.A. et al. (2002) "Dilysine trigger" in transferrins probed by mutagenesis of lactoferrin: crystal structures of the R210G, R210E, and R210L mutants of human lactoferrin. *Biochemistry* 41 (48), 14167-14175
- 67 D.R. Hall, J.M.H., G.A. Leonard, S. Bailey, M. Neu, M. Winn and P.F. Lindley. (2001) The Crystal and Molecular Structures of Differeic Porcine and Rabbit Serum Transferrins at Resolutions of 2.15 and 2.60 Angstroms, Respectively. *Acta Crystallographics Section D* D58, 70-80
- 68 MacGillivray, R.T. et al. (1998) Two high-resolution crystal structures of the recombinant N-lobe of human transferrin reveal a structural change implicated in iron release. *Biochemistry* 37 (22), 7919-7928
- 69 Bohrmann, B. et al. (1999) Endogenous proteins controlling amyloid beta-peptide polymerization. Possible implications for beta-amyloid formation in the central nervous system and in peripheral tissues. *J Biol Chem* 274 (23), 15990-15995
- 70 Dautry-Varsat, A. et al. (1983) pH and the recycling of transferrin during receptor-mediated endocytosis. *Proc Natl Acad Sci U S A* 80 (8), 2258-2262

- 71 Vogel, W. et al. (1989) Occupancy of the iron-binding sites of human transferrin in sera obtained from different anatomical sites. *Klin Wochenschr* 67 (10), 538-542
- 72 Narayanan, S. and Reif, B. (2005) Characterization of chemical exchange between soluble and aggregated states of beta-amyloid by solution-state NMR upon variation of salt conditions. *Biochemistry* 44 (5), 1444-1452
- 73 Narayanan, S. et al. (2003) Importance of low-oligomeric-weight species for prion propagation in the yeast prion system Sup35/Hsp104. *Proc Natl Acad Sci U S A* 100 (16), 9286-9291
- 74 Furihata, K. et al. (2008) An efficient use of the WATERGATE W5 sequence for observing a ligand binding with a protein receptor. *Magn Reson Chem* 46 (9), 799-802
- 75 Piotto, M. et al. (1992) Gradient-tailored excitation for single-quantum NMR spectroscopy of aqueous solutions. *J Biomol NMR* 2 (6), 661-665
- 76 Huang, H. et al. (2008) Analysis and optimization of saturation transfer difference NMR experiments designed to map early self-association events in amyloidogenic peptides. *J Phys Chem B* 112 (18), 5795-5802
- 77 Julijana Milojevic, V.E., Rahul Das and Giuseppe Melacini. (2006) Analysis and Parametric Optimization of ¹H Off-Resonance Relaxation NMR Experiments Designed to Map Polypeptide Self-Recognition and Other Noncovalent Interactions. *Journal of Physical Chemistry* 110, 20664-20670
- 78 Esposito, V. et al. (2005) Mapping polypeptide self-recognition through (1)H off-resonance relaxation. *J Am Chem Soc* 127 (26), 9358-9359
- 79 Meyer, M.M.a.B. (1999) Characterization of Ligand Binding by Saturation Transfer Difference NMR Spectroscopy. *Angewandte Chemie International Edition* 38 (12), 1784-1788
- 80 Klement, K. et al. (2007) Effect of different salt ions on the propensity of aggregation and on the structure of Alzheimer's abeta(1-40) amyloid fibrils. *J Mol Biol* 373 (5), 1321-1333
- 81 Subramaniam, S. (2008) The Biology WorkBench 3.2. University of Illinois National Center for Supercomputing Applications
- 82 Gill, S.C. and von Hippel, P.H. (1989) Calculation of protein extinction coefficients from amino acid sequence data. *Anal Biochem* 182 (2), 319-326
- 83 Milojevic, J. et al. (2007) Understanding the molecular basis for the inhibition of the Alzheimer's Abeta-peptide oligomerization by human serum albumin using saturation transfer difference and off-resonance relaxation NMR spectroscopy. *J Am Chem Soc* 129 (14), 4282-4290
- 84 Goddard, T. (2006) Sparky 3.111. (Kneller, D., ed.)
- 85 Benjamin M. Bulheller, A.R.a.J.D.H. (2007) Circular and Linear Dichroism of Proteins. *Physical Chemistry Chemical Physics* 9, 2020-2035
- 86 Sergio Guitna, R.G., M. Beatrice Valli, Elizabeth H. Corder, Luciano Galeazzi. (2004) Transferrin Neutralization of Amyloid β 25-35 Cytotoxicity. *Clinica Chimica Acta* 350, 129-136

- 87 Loeffler, D.A. et al. (1995) Transferrin and iron in normal, Alzheimer's disease, and Parkinson's disease brain regions. *J Neurochem* 65 (2), 710-724
- 88 Barnham, K.J. and Bush, A.I. (2008) Metals in Alzheimer's and Parkinson's diseases. *Curr Opin Chem Biol* 12 (2), 222-228
- 89 Hu, W.P. et al. (2006) Kinetic analysis of beta-amyloid peptide aggregation induced by metal ions based on surface plasmon resonance biosensing. *J Neurosci Methods* 154 (1-2), 190-197
- 90 Evan, K. et al. (1995) Whole systems shared governance: a model for the integrated health system. *J Nurs Adm* 25 (5), 18-27
- 91 Wüthrich, K. (1986) *NMR of Protein and Nucleic Acids*, A Wiley-Interscience Publication
- 92 Huang, X. et al. (1999) The A beta peptide of Alzheimer's disease directly produces hydrogen peroxide through metal ion reduction. *Biochemistry* 38 (24), 7609-7616
- 93 Bertini, I. et al. (2005) NMR spectroscopy of paramagnetic metalloproteins. *Chembiochem* 6 (9), 1536-1549
- 94 Bertini, I. et al. (2005) NMR spectroscopic detection of protein protons and longitudinal relaxation rates between 0.01 and 50 MHz. *Angew Chem Int Ed Engl* 44 (15), 2223-2225
- 95 Welch, S. (1992) *Transferrin: The Iron Carrier*, CRC Press
- 96 Galeazzi, L. et al. (2002) Albumin protects human red blood cells against Aβ₂₅₋₃₅-induced lysis more effectively than ApoE. *Neuroreport* 13 (16), 2149-2154